This paper is available on line at http://www.mcponline.org

Integrated Stable Isotope Labeling by Amino Acids in Cell Culture (SILAC) and Isobaric Tags for Relative and Absolute Quantitation (iTRAQ) Quantitative Proteomic Analysis Identifies Galectin-1 as a Potential Biomarker for Predicting Sorafenib Resistance in Liver Cancer*[S]

Chao-Chi Yeh‡, Chih-Hung Hsu§‖, Yu-Yun Shao§‖, Wen-Ching Ho‡, Mong-Hsun Tsai¶, Wen-Chi Feng‡, and Lu-Ping Chow‡**

Sorafenib has become the standard therapy for patients with advanced hepatocellular carcinoma (HCC). Unfortunately, most patients eventually develop acquired resistance. Therefore, it is important to identify potential biomarkers that could predict the efficacy of sorafenib. To identify target proteins associated with the development of sorafenib resistance, we applied stable isotope labelling with amino acids in cell culture (SILAC)-based quantitative proteomic approach to analyze differences in protein expression levels between parental HuH-7 and sorafenib-acquired resistance HuH-7 (HuH-7^R) cells *in vitro*, combined with an isobaric tags for relative and absolute quantitation (iTRAQ) quantitative analysis of HuH-7 and HuH-7^R tumors *in vivo*. In total, 2,450 quantified proteins were identified in common in SILAC and iTRAQ experiments, with 81 showing increased expression (>2.0-fold) with sorafenib resistance and 75 showing decreased expression (<0.5-fold). *In silico* analyses of these differentially expressed proteins predicted that 10 proteins were related to cancer with involvements in cell adhesion, migration, and invasion. Knockdown of one of these candidate proteins, galectin-1, decreased cell proliferation and metastasis in HuH-7^R cells and restored sensitivity to sorafenib. We verified galectin-1 as a predictive marker of sorafenib resistance and a downstream target of the AKT/mTOR/HIF-1α signaling pathway. In addition, increased galectin-1 expression in HCC patients' serum was associated with poor tumor control and low response rate. We also found that a high serum galectin-1 level was an independent factor associated with poor progression-free survival and overall survival. In conclusion, these results suggest that galectin-1 is a possible biomarker for predicting the response of HCC patients to treatment with sorafenib. As such, it may assist in the stratification of HCC and help direct personalized therapy. ***Molecular & Cellular Proteomics 14: 10.1074/mcp.M114.046417, 1527–1545, 2015.***

Hepatocellular carcinoma (HCC)[1] is one of the most common cancers in the world and the third-most frequent cause of cancer deaths. Notably, the incidence of HCC is highest in Asia and Africa (1). Currently, 30% to 40% of patients are diagnosed at early stages and are suitable for curative treatments or locoregional procedures (2). However, a majority of HCC patients presents with advanced-stage tumors and require systemic therapy; previous progress in systemic therapy for advanced HCC has been limited (3, 4).

Sorafenib, which can prolong the overall survival of patients with inoperable, advanced HCC by 6–9 months, is currently

From the ‡Graduate Institute of Biochemistry and Molecular Biology, §Graduate Institute of Oncology, College of Medicine, ¶Institute of Biotechnology, National Taiwan University and ‖Department of Oncology, National Taiwan University Hospital, Taipei, Taiwan

Received, November 11, 2014 and in revised form, February 24, 2015

Published, MCP Papers in Press, April 7, 2015, DOI 10.1074/mcp.M114.046417

Author contributions: C.H. and L.C. designed research; C.Y., W.H., and W.F. performed research; C.Y., Y.S., and M.T. analyzed data; C.Y., C.H., and L.C. wrote the paper.

[1] The abbreviations used are: HCC, hepatocellular carcinoma; HuH-7, human hepatocellular carcinoma cell line; SILAC, stable isotope labeling by amino acids in cell culture; iTRAQ, isobaric tags for relative and absolute quantitation; 2D-LC-MS/MS, two-dimensional liquid chromatography tandem mass spectrometry; EMT, epithelial-mesenchymal transition; IPA, Ingenuity Pathway Analysis; AKT/PI3K, protein kinase B/phosphatidylinositol 3-kinase; mTOR, mammalian target of rapamycin; CTGF, connective tissue growth factor; IQGAP1, IQ motif-containing GTPase-activating protein 1; EPHA2, EPH receptor A2.

the only effective systemic drug for such patients. Sorafenib is a multikinase inhibitor that targets Raf kinase, vascular endothelial growth factor receptor (VEGFR) and platelet-derived growth factor receptor (PDGFR), showing activity against both tumor cell proliferation and tumor angiogenesis (5). In the pivotal SHARP study and subsequent Asia-Pacific Study, sorafenib improved the median overall survival by 2–3 months in patients with advanced HCC (3, 6). Despite this significant improvement in survival, the efficacy of sorafenib against HCC is modest, with an objective tumor response rate as low as 2% to 3% (3). In other words, many HCC patients are inherently resistant to sorafenib. For those who show an initial response or stabilization to sorafenib, disease progression inevitably ensues, indicating development of acquired resistance. Therefore, it is imperative to identify biomarkers that can predict the efficacy of sorafenib and outcomes in advanced HCC patients. Further, targeting drug resistance mechanisms of sorafenib may lead to the development of novel strategies to improve the efficacy of sorafenib in HCC.

Mass spectrometry-based proteomic technology is currently used to study and compare the proteomes of *in vitro* and *in vivo* models of cancer as well as patient tumors, and has opened up new avenues for tumor-associated biomarker discovery. A number of studies have employed this tool to examine drug resistance, and have revealed significant differences in the expression of proteins associated with key biological processes, such as cell proliferation, survival, and motility (7). Because they facilitate the simultaneous analysis of whole proteomes, proteomic technologies have led to the identification of various biomarkers associated with resistance to anticancer therapy (8). A number of studies have sought to identify tumor and/or plasma biomarkers that could be used to predict clinical benefit for patients with advanced HCC receiving sorafenib therapy (9). Changes in biomarker concentrations during treatment may predict drug response and provide insights into mechanisms of drug action or patient resistance. There is thus an urgent need to identify predictive biomarkers that could exclude advanced HCC patients who are unlikely to benefit from sorafenib therapy.

In the present study, we used quantitative proteomics to analyze parental HuH-7 and sorafenib-acquired resistance HuH-7^R HCC cell lines using the stable isotope labeling with amino acid in cell culture (SILAC) approach. We further extended this approach by incorporating HCC xenograft models using isobaric tags for relative and absolute quantitation (iTRAQ) quantitative analysis. This approach allowed the identification of 10 proteins involved in cell motility or invasion processes that were differentially expressed between HuH-7 and HuH-7^R cells. Among these proteins, galectin-1 was identified as a predictive marker for sorafenib resistance and a downstream target of the AKT/mTOR/HIF-1α signaling pathway. These results reveal a new role for galectin-1 in sorafenib resistance that could be of therapeutic value in the detection of sorafenib-resistant HCCs. We believe that the results of this study could provide additional insight into the mechanisms underlying the sensitivity and resistance to sorafenib in HCC cells. This, in turn, may help identify possible novel therapeutic targets, as well as biomarkers that aid patient stratification for optimal therapy.

EXPERIMENTAL PROCEDURES

Cell Lines, Tumor Models, and Transfection—The HCC HuH-7 cell line was obtained from the Health Science Research Resources Bank (JCRB0403, Osaka, Japan). The sorafenib-resistant HCC cell line, HuH-7^R, was established by long-term exposure of cells to sorafenib as previously reported (10).

The Institutional Laboratory Animal Care and Use Committee of National Taiwan University approved the animal studies. The tumor xenograft model was prepared by subcutaneously injecting 5×10^6 HuH-7 or HuH-7^R cells into 5-week-old BALB/c nude mice. Tumor dimensions were measured with a caliper at 3-day intervals, and tumor volume was calculated as length $\times$ width $\times$ height (in cm^3). For the tail vein inoculation model, 1×10^6 HuH-7 or HuH-7^R cells were injected by tail vein and mice were sacrificed after 6 weeks. Paraffin-embedded, hematoxylin and eosin (H&E)-stained lung sections were analyzed microscopically for tumor nodules.

Target sequences used for galectin-1 knockdown experiments are listed in supplemental Table S1. Lentiviruses expressing small hairpin (inhibitory) RNA (shRNA) against galectin-1 (shGal-1) or control shRNA (shCtrl) was produced in HEK293FT cells. Medium containing shGal-1 or shCtrl viruses was applied to cultures of HuH-7 and HuH-7^R cells. Cell-proliferation, wound-healing, and invasion assays were performed after transduction of cells with shRNA-expressing viruses.

Cell Proliferation, Wound-healing, and Invasion Assays—Cell viability was measured using MTT [3-{4,5-dimethylthiazol-2-yl}-2,5- diphenyltetrazolium bromide] assays; cell migration was assessed with a scratch wound-healing assay using a Boyden chamber; and the invasive capability of cells was determined using Matrigel-coated invasion chambers, as described previously (11).

Sample Preparation—For SILAC, HuH-7^R cells were heavy labeled by culturing in Dulbecco's Modified Eagle Medium (DMEM) [$^{13}C_6$]-L-lysine and [$^{13}C_6$, $^{15}N_4$]-L-arginine (Invitrogen, Carlsbad). HuH-7 cells were maintained in the same medium containing unlabeled amino acids. Labeled HuH-7 and HuH-7^R cells were washed with PBS to remove serum proteins and then scraped in lysis buffer containing 25 mM Tris-HCl, pH 7.6, 150 mM NaCl, 1% Nonidet P-40, 1% sodium deoxycholate, 0.1% SDS, and protease inhibitors (Pierce, Rockford). The lysate was sonicated and centrifuged to pellet cellular debris. Equal amounts of SILAC proteins were mixed, reduced and alkylated by incubating with 5 mM dithiothreitol (DTT) for 60 min and 10 mM Iodoacetamide (IAA) for 60 min, followed by a 15-min IAA-neutralizing step. Proteins were digested with trypsin (1:100, w/w) (Promega, Madison) at 37 °C overnight. Trifluoroacetic acid was added to a concentration of 0.4% to terminate the digestion reaction.

For iTRAQ, total protein was extracted from xenograft tumors formed from HuH-7 or HuH-7^R tumors ($n = 6$ each) and enriched using a 3-kDa centrifugal filter (Millipore, Watford, UK). This process was repeated twice using double-distilled H_2O to desalt and remove the protease inhibitor mixture. A total of 400 μg of protein was collected from paired HuH-7 and HuH-7^R tumors for iTRAQ analysis. The protein mixtures were incubated in 0.5 M triethylammonium bicarbonate (TEAB; pH 8.5) and 2% SDS, reduced with 5 mM Tris (2-carboxyethyl) phosphine (TCEP) for 1 h at 60 °C, and alkylated with 10 mM s-methyl methanethiosulfonate (MMTS) at room temperature for 10 min. Each 100 μg of protein was digested overnight in tryptic solution (1:100) at 37 °C. Digested peptides from HuH-7 and

HuH-7^R tumors were labeled with 114,115 and 116,117 iTRAQ reagents (SCIEX, Foster City), respectively.

Off-line 2D-LC-MS/MS—Equally mixed SILAC and iTRAQ peptides were injected into a basic C18 column (Zorbax, 300 Extend-C18, 5 μm, 4.6 $\times$ 150 mm; Agilent, Santa Clara) and fractionated into 24 fractions using a continuous acetonitrile gradient in the presence of 10 mM ammonia bicarbonate and 5% acetonitrile (pH 10). The basic reverse phase-HPLC buffers consisted of buffer A (10 mM NH_4HCO_3 in 5% acetonitrile, pH 10) and buffer B (10 mM NH_4HCO_3 in 90% acetonitrile, pH 10). The gradient was 0–10% buffer B for 5 min, 10–30% buffer B for 25 min, 30–100% buffer B for 15 min, hold in 100% buffer B for 5 min, and then equilibrate with buffer A for 10 min.

Each fraction was trapped on a reverse phase C18 column (Acclaim PepMap100, 3 μm, 100 Å, 75 μm $\times$ 2 cm; Dionex, Sunnyvale) and separated using coupled reverse phase C18 chromatography (Acclaim PepMap RSLC, 2 μm, 100 Å, 75 μm $\times$ 15 cm; Thermo Fisher Scientific, Waltham) with an acetonitrile gradient in 0.1% formic acid. The injection volume was 2 μl, and the flow rate was 250 nL/min. The mobile phases consisted of buffer A (0.1% formic acid) and buffer B (0.1% formic acid in 90% acetonitrile). The gradient condition was 4–30% buffer B for 90 min, 30–90% buffer B for 15 min, hold in 90% buffer B for 10 min, and then equilibrate with buffer A for 15 min. Full-scan MS spectra (m/z 300–1600) were acquired in an Orbitrap mass analyzer at a resolution of 60,000. The lock mass calibration feature was enabled to improve mass accuracy, with lock mass set at 445.12003 (polycyclodimethylsiloxane).

For SILAC analysis, the most intense ions (up to 20) with a minimal signal intensity of 1000 were sequentially isolated for MS/MS fragmentation in order of the intensity of precursor peaks in the linear ion trap using a collision-induced dissociation energy of 30%, Q activation at 0.25, an activation time of 10 ms, and an isolation width of 2.0. Targeted ions with *m/z* $\pm$ 10 ppm were selected for MS/MS and dynamically excluded for 60 s.

For iTRAQ analysis, MS data were acquired using the following parameters: 10 data-dependent CID-HCD dual MS/MS scans per full scan; CID scans acquired in LTQ with two-microscan averaging; full scans and HCD scans acquired in Orbitrap at a resolution of 60,000 and 15,000, respectively; normalized collision energy (NCE) of 30% in CID and 50% in HCD; $\pm$ 2.0 *m/z* isolation window; and dynamic exclusion for 60 s. In CID-HCD dual scan, each selected parent ion was first fragmented by CID and then by HCD.

Protein Identification and Quantification—The precursor mass tolerance was set at 7 ppm, and fragment ion mass tolerance set at 0.5 Da. The dynamic modifications were deamidated (NQ), oxidation (M), and N-terminal acetylation. The static modification was cysteine carbamidomethylation, and a maximum of two miscleavages were allowed. False discovery rate was calculated by enabling the peptide sequence analysis using a decoy database. Identified peptides were validated using a Percolator algorithm with a q-value threshold of 0.01. Mass spectrometry data were processed and quantified using Proteome Discoverer (Version 1.3) software (Thermo Fisher Scientific) workflow from the Mascot search engine (version 2.3.02), and searched against the Swiss-Prot 57.2 version with *Homo sapiens* (human) protein database containing 20,232 sequences.

For SILAC-based proteomics, the search parameters were set using isotope labeling of lysine (+6.020 Da) and isotope labeling of arginine (+10.008 Da) as the dynamic modifications. For each SILAC pair, Proteome Discoverer determines the area of the extracted ion chromatogram and computes the "heavy/light" ratio. Protein ratios are then calculated as the median of all the quantified unique peptides belonging to a certain protein. The ratios among proteins in the heavy and light versions were used as fold-change.

For iTRAQ-based proteomics, the search parameters were set using methyl methanethiosulfonate as cysteine, iTRAQ 4-plex at lysine, and the N-terminal residue as static modifications. Fragment ion mass tolerance and precursor ion tolerance were set to 0.2 Da with a 95% confidence threshold.

Bioinformatics Analysis—Data sets representing proteins with altered expression profile derived from quantitative proteomics (SILAC and iTRAQ) analyses were categorized into functional groups based on the Ingenuity Pathway Analysis Tool (Ingenuity Systems, Redwood City; http://www.ingenuity.com). In IPA, differentially expressed proteins are analyzed in terms of biological responses and canonical pathways. Ranking and significance of the bio-functions and the canonical pathways were tested by the *p* value. The bio-functions and canonical pathways were ordered by the ratio (numbers of genes from the input data set that map to the pathway divided by the total number of molecules that exist in the canonical pathway). Additionally, differentially expressed proteins are mapped to gene networks available in the Ingenuity database and then ranked by score. The networks created are ranked depending on the number of significantly expressed genes they contain; the most significant associated diseases are also listed. A network is a graphical representation of the molecular relationships among these molecules. Genes or gene products are represented as nodes, and the biological relationship between two nodes is represented as an edge (line). All edges are supported by at least one literature reference and canonical information stored in the Ingenuity Pathways Knowledge Base. The intensity of the node color indicates the expression level of up-regulation (red) or down-regulation (green).

Immunoblotting and Immunohistochemistry (IHC)—A total of 17 commercial antibodies were used for Western blotting, including antibodies to vimentin, CTGF, IQGAP1, galectin-1, ezrin, annexin A2, E-cadherin, 4EBP1, S65-phosphorylated 4EBP1 (p4EBP1), P70S6K, T389-phosphorylated P70S6K (pP70S6K), S6, S235/236-phosphorylated S6 (pS6), AKT, S473-phosphorylated AKT (pAKT), HIF-1α, and β-actin. Except for antibodies against galectin-1 (Abcam, Cambridge, UK), E-cadherin, AKT/pAKT (Santa Cruz Biotechnology, Santa Cruz) and CTGF/ezrin/annexin A2 (GeneTex, Irvine), all antibodies were purchased from Cell Signaling Technology, Hitchin, UK. Anti-galetin-1 and Ki-67 antibodies from Santa Cruz and Dako, Glostrup, Denmark, respectively, were used for immunohistochemistry. Immunoblotting and immunohistochemistry analyses were done as described previously (12).

Reverse Transcription-polymerase Chain Reaction (RT-PCR) and Chromatin Immunoprecipitation (ChIP) Assays—The expression of galectin-1 mRNA was quantified by RT-PCR using β-actin as an internal standard for normalization. For ChIP assays, cells were grown under normoxia or treated with $CoCl_2$ and then cross-linked and quenched. Subsequently, cells were lysed and sonicated, yielding 200–1000 bp DNA fragments. ChIP assays were performed using the SimpleChIP Enzymatic Chromatin IP Kit (Cell Signaling). The specific primers used for RT-PCR and ChIP are shown in supplemental Table S1.

Quantification of Galectin-1 in Patient Serum—A total of 91 HCC patients who received sorafenib-based treatment as the first-line therapy for advanced HCC from 2007 to 2012 and who consented to having their peripheral blood collected for analysis before the treatment started were enrolled in this study. The study was approved by the Institute Research Ethical Committee of National Taiwan University Hospital.

Serum levels of galectin-1 were determined with a galectin-1 sandwich enzyme-linked immunosorbent assay (ELISA). In brief, 96-well microplates (PerkinElmer, Shelton) were precoated with galectin-1 capture antibody (AF1152; R&D Systems, Minneapolis) at 4 °C overnight. After washed, the plate was treated with blocking buffer (Block-PRO Blocking buffer; Visual Protein, Taipei, Taiwan) at 37 °C for 1 h. Plates were then washed, and serum samples (100 μl) were added

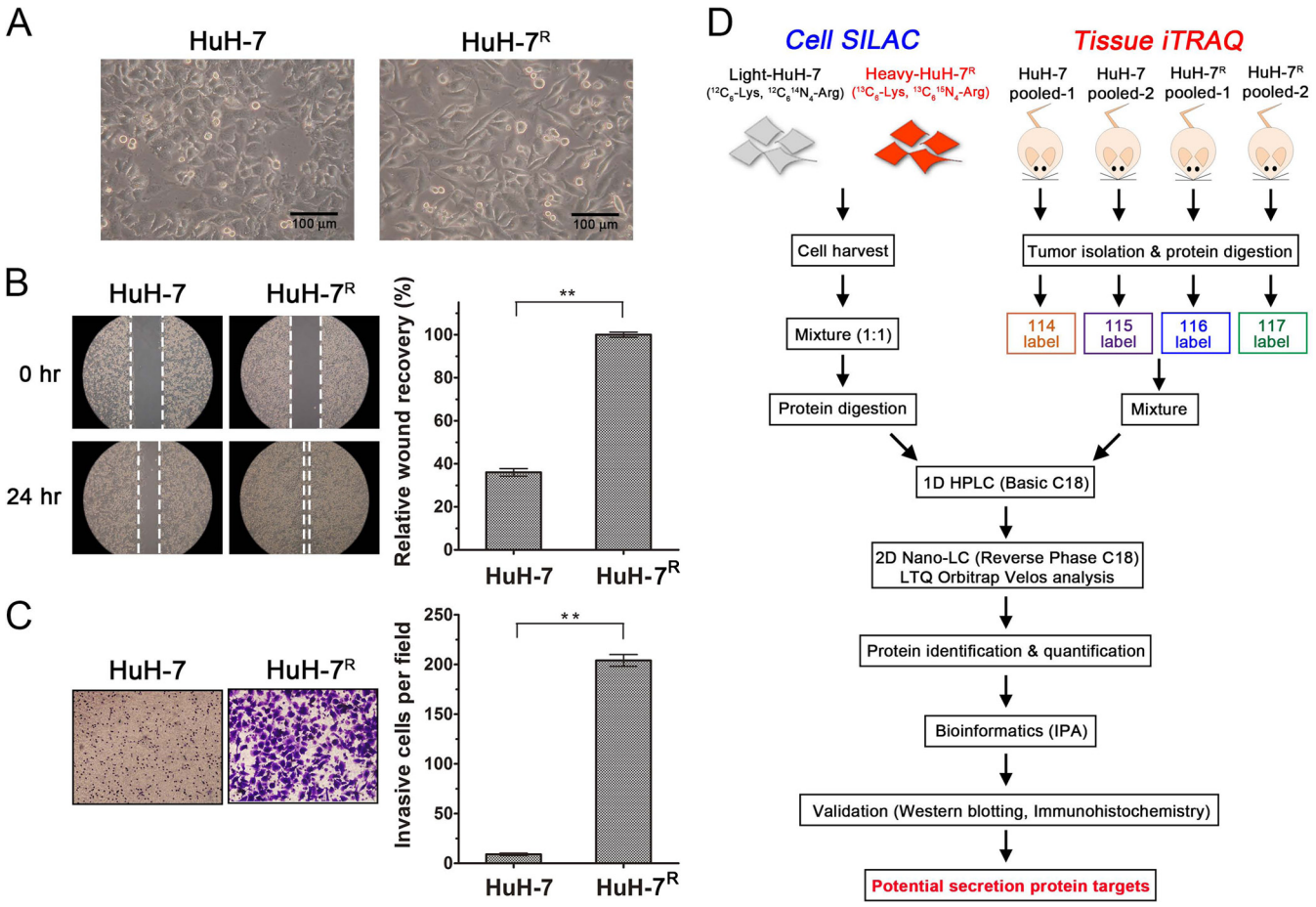

FIG. 1. **Experimental set-up for analyzing sorafenib-induced differentially, protein expression profiles in liver cancer models.** *A*, Cell morphology is different between parental HuH-7 cells (left) and sorafenib-resistant HuH-7^R cells (right). *B*, Wound-healing assays of HuH-7 and HuH-7^R cells. The micrographs show cells that had migrated into the gap 0 and 24 h after removal of the insert. *C*, Transwell migration assays of HuH-7 and HuH-7^R cells. Cells in the central field of each insert were visualized by light microscopy and quantified. Data are presented as means ± S.D. *D*, Schematic overview of the strategies used for the SILAC and iTRAQ analyses. Cell lines or tissues were harvested under denaturing conditions, digested with trypsin, separated on a column, and run on an LTQ-Orbitrap Velos hybrid mass spectrometer.

and further incubated at 37 °C for 2 h. Thereafter, biotinylated galectin-1 detection antibody (BAF1152; R&D Systems) was added and incubated at 37 °C for 2 h. The wells were then rinsed and 100 µl of a solution containing streptavidin-horseradish peroxidase (1:200) was added. After 1 h incubation, plates were washed and an NeA-Blue (tetramethylbenzidine substrate; Clinical Science Product Inc., Massachusetts) solution was added to the wells; the reaction was stopped by adding 1 mol/L H_2SO_4. The absorbance of each sample was determined at 450 nm. A standard curve prepared from 5 to 120 ng of galectin-1 was generated for each ELISA.

Statistical Analysis—Statistical analyses were conducted using SAS software. An independent *t* test was utilized to compare serum galectin-1 levels between healthy volunteers and patients. The associations between high or low galectin-1 levels and disease control or other baseline characteristics as nominal variables were analyzed using the Chi-square test or Fisher's exact test. Progression-free survival and overall survival were estimated using the Kaplan-Meier method and compared using with a log-rank test. In multivariate analyses, the Cox proportional hazards regression model was used to adjust for other potential clinicopathologic parameters described elsewhere (13). All tests were two-sided, and a p value ≤ 0.05 was considered statistically significant.

RESULTS

Functional Analyses of HuH-7 and HuH-7^R Cells—Resistant HuH-7^R cell lines were established previously (10). As shown in supplemental Fig. S1, the IC_{50} value for sorafenib against these cells (8.75 µM) is shifted to a higher value compared with that against HuH-7 cells (4.13 µM). HuH-7 cells grew in monolayer clusters, whereas HuH-7^R cells adopted a spindle shape and lost cell–cell contact, suggesting that resistant cells display a more mesenchymal phenotype (Fig. 1*A*). To further confirm these observations, we performed wound-healing and invasion assays, which revealed that migration rate (Fig. 1*B*) and invasiveness (Fig. 1*C*) were dramatically increased in HuH-7^R cells compared with HuH-7 cells. These data suggest that HuH-7^R cells possess a more aggressive phenotype than HuH-7 cells.

Identification and Quantification of Differentially Expressed Proteins in HuH-7 and HuH-7^R Cells and Cell-Derived Tumors—To elucidate the differentially expressed proteins in

sorafenib resistant HuH-7^R cells compared with parental HuH-7 cells, we utilized two different quantitative proteomic analyses: SILAC (for *in vitro* labeling) and iTRAQ (for *in vivo* labeling). A schematic diagram of the experimental design for exploring sorafenib-acquired resistance in HuH-7 cells is shown in Fig. 1*D*. SILAC-based proteomic analysis yielded a total of 4,616 quantified proteins in both forward and reverse experiments, which could avoid biases in cell labeling. Of these proteins, 699 were found to have statistically significant changes in expression in the HuH-7^R cells (supplemental Fig. S2). To further determine the *in vivo* response to sorafenib resistance, a total of 2,836 proteins were successfully identified and quantified using iTRAQ-based proteomic analysis. Outliers were identified based on a p value > 0.05 and 114/116 and 115/117 ratio >2.0 or < 0.5. This resulted in 567 proteins being considered statistically reliable hits (supplemental Fig. S2). Among those data sets, a total of 2,450 proteins common to both SILAC and iTRAQ experiments were reliably (false discovery rate [FDR] $< 1\%$) identified and quantified. Ultimately, quantitative data from both data sets were normalized against the 5% trimmed means to minimize the effect of extreme outliers and to center the protein $\log_2$ ratio distribution on zero (14).

Biological Function, Pathway, and Network Analysis—An analysis of the abundance of proteins in SILAC and iTRAQ data sets showed that 156 proteins were differentially expressed between HuH-7 and HuH-7^R cells: expression of 81 proteins was increased in HuH-7^R cells (>2.0-fold), and expression of 75 proteins was decreased (<0.5-fold) (Fig. 2*A* and Table I, II). For a few proteins with only one quantified peptide, MS and MS/MS spectra were manually inspected to avoid error erroneous quantification (supplemental Fig. S3). To identify altered biological functions that might play a role in sorafenib resistance, we further analyzed the 156 quantified proteins using the functional analysis of up-regulated proteins, which were mainly related to cellular movement ($n = 9$), cellular growth and proliferation ($n = 19$), cellular development ($n = 19$) and cellular assembly and organization ($n = 11$) (Fig. 2*B* and Supplemental Table S2); whereas the down-regulated proteins were predominantly involved in amino acid metabolism ($n = 7$), small molecule biochemistry ($n = 7$) and nucleic acid metabolism ($n = 8$) (Fig. 2*B* and supplemental Table S2). IPA was further adopted for grouping proteins into networks and canonical pathways to determine the altered cellular activities during sorafenib resistance. The top one network associated with up-regulated proteins was found to be mainly involved in cellular movement, cell-to-cell signaling and interaction and tissue development. On the contrary, the top networks of down-regulated proteins involved in drug metabolism, endocrine system development and function (Table III). Additionally, the most significant biological network, which received an IPA score 47, included several differentially expressed proteins that correlated with the PI3K/AKT and mTOR signaling pathways (Fig. 2*C*). Among those proteins were simultaneously associated with different biological functions and disease, such as metastasis, formation of cellular protrusions, liver cancer, and proliferation of tumor cells (Fig. 2*C* and Table IV). In summary, we found 10 significantly differentially expressed proteins identified in proteomic data – annexin A1 (ANXA1), annexin A2 (ANXA2), coiled-coil domain-containing 88A; gridin (CCDC88A), connective tissue growth factor (CTGF), EPH receptor A2 (EPHA2), ezrin (EZR), galectin-1 (LGALS1), IQ motif-containing GTPase-activating protein 1 (IQGAP1), Ral GTPase-activating protein, alpha subunit 2 (RALGAPA2), and vimentin (VIM), which mainly participated in cellular movement. These finding led us to focus on proteins that could play a relevant role in cell motility and metastasis.

Selected In Vitro- and In Vivo-Overexpressed Proteins Associated with Epithelial-Mesenchymal Transition (EMT)—A set of six out of the 10 candidate proteins associated with EMT including vimentin, CTGF, IQGAP1, galectin-1, ezrin, and annexin A2, were selected. MS spectra of representative peptides are shown in Fig. 3 and these proteins were further validated by Western blotting analysis. The SILAC-based quantitative MS spectrum was consistent with the iTRAQ-based quantitative MS spectrum. Western blotting results were consistent with those of proteome analysis (supplemental Fig. S4). To further identify proteins dysregulated in HuH-7^R cells that might be used as HCC serum biomarkers for predicting sorafenib resistance, we analyzed quantified proteins using the SignalP program. A total of 22 proteins were putative secreted proteins; two of these candidates—galectin-1 and CTGF—were highly expressed in HuH-7^R cells. Interestingly, galectin-1, which was significantly up-regulated in HuH-7^R cells and is known to play a crucial role in the regulation of cell migration, was identified in HuH-7^R cell conditioned medium, confirming that it was secreted (supplemental Fig. S5). In contrast, CTGF was not detected in conditioned medium (data not shown).

Galectin-1 Knockdown Inhibits HuH-7^R Cell Proliferation, Migration, and Invasion, and Restores Sorafenib Sensitivity—We next sought to investigate the role of galectin-1 in conferring sorafenib resistance and increasing migration. Because HuH-7 cells expressed negligible levels of galectin-1 compared with HuH-7^R cells, we employed lentiviral-mediated delivery of galectin-1 shRNAs to inhibit the expression of galectin-1 in HuH-7^R cells (Fig. 4*A*). Transduction of HuH-7^R cells with shGal-1 dramatically decreased galectin-1 expression (Fig. 4*B*). Subsequent MTT assays showed that knockdown galectin-1 significantly suppressed proliferation in HuH-7^R cells (Fig. 4*C*). Wound-healing and invasion assays performed in galectin-1-knockdown HuH-7^R cells revealed that suppression of galectin-1 expression significantly blocked migration ability (Fig. 4*D*) and invasion activity (Fig. 4*E*) compared with HuH-7^R cells. Importantly, we found that repression of galectin-1 restored sorafenib sensitivity in HuH-7^R cells (Fig. 4*F*), reducing the IC_{50} of sorafenib to a

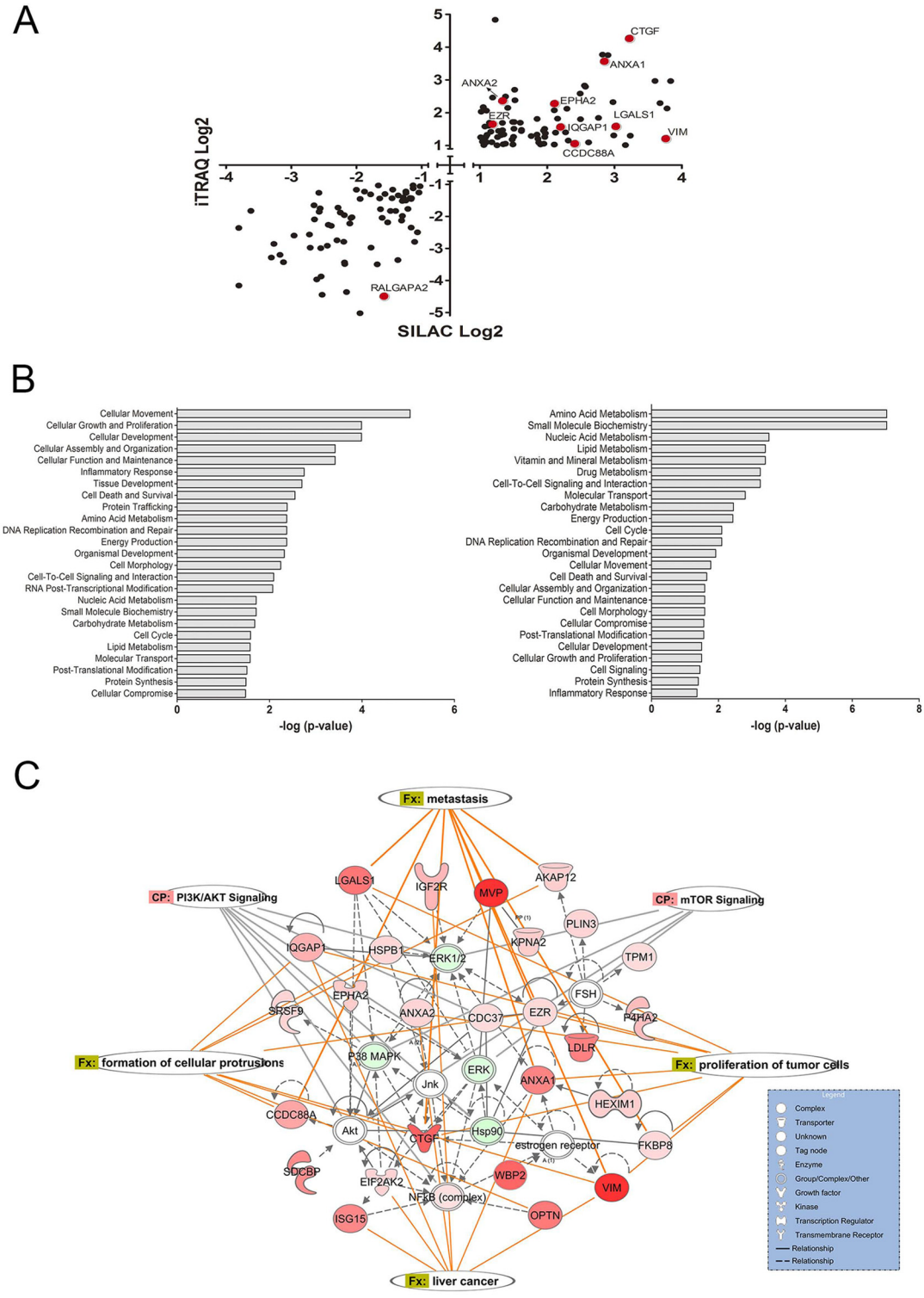

FIG. 2. **Analysis of proteins differentially expressed between HuH-7^R and HuH-7 cells *in vitro* (SILAC) and tumors *in vivo* (iTRAQ).** *A*, Scatter plot showing at least twofold changes in both SILAC and iTRAQ experiments. Red spots represent EMT-related proteins. The 156 differentially expressed proteins were analyzed using functional analysis in IPA. *B*, Graphical demonstration of associated functions from up-regulated proteins (left panel) and down-regulated proteins (right panel). The *y* axis displays the functional categories that are identified in analyses. The *x* axis shows the significance, which is the value of −log (P). *C*, Top-scored biological network analysis implicated that sorafenib induces cell migration and metastasis. Associations among proteins are shown by solid or dashed lines, which represent direct and indirect interactions, respectively. Up-regulated proteins are shown in red, and down-regulated proteins are shown in green. Four proteins found by IPA data mining tools are shown in gray.

TABLE I
Up-regulated proteins (fold change > 2.0) in HuH-7^R cells

Accession number	Description	Symbol	Coverage (%)	Match peptides	H/L ratio	Mascot scores	Coverage (%)	Match peptides	116/114 ratio[a]	Mascot scores	Metastasis
O60831	PRA1 family protein 2	PRAF2	6.18	1	14.27	80.33	10.11	1	7.82	52.87	
P43362	Melanoma-associated antigen 9	MAGA9	24.76	7	13.74	768.79	2.54	1	4.39	20.0	
P08670	Vimentin	VIM	66.95	36	13.64	10915.40	55.36	27	2.29	2727.24	√
Q14764	Major vault protein	MVP	38.19	25	12.79	2069.64	16.35	14	4.90	449.43	
P07195	L-lactate dehydrogenase B chain	LDHB	45.21	14	12.14	2477.52	31.74	12	7.83	503.91	
Q01813	6-phosphofructokinase type C	PFKP	42.60	26	9.41	2340.67	18.49	15	2.46	408.53	
P29279	Connective tissue growth factor	CTGF	7.45	1	9.33	166.02	10.03	3	19.00	75.08	√
Q969T9	WW domain-binding protein 2	WBP2	17.24	1	8.96	121.30	6.13	2	2.02	31.00	
P09382	Galectin-1	LGALS1	76.30	7	8.13	1892.21	23.70	3	2.97	309.40	√
P08237	6-phosphofructokinase, muscle type	PFKM	26.92	13	7.94	991.35	9.74	9	2.48	91.65	
Q96CV9	Optineurin	OPTN	9.36	4	7.88	289.11	3.81	3	5.00	32.84	
P01130	Low-density lipoprotein receptor	LDLR	4.53	3	7.47	183.69	1.51	1	13.52	114.70	
P04083	Annexin A1	ANXA1	59.54	22	7.23	4682.62	45.95	17	11.80	2416.09	√
P05161	Ubiquitin-like protein ISG15	ISG15	38.79	5	7.07	643.24	34.55	6	13.64	66.15	
O00560	Syntenin-1	SDCBP	40.27	6	6.78	853.92	6.71	1	3.59	33.10	
O14657	Torsin-1B	TOR1B	6.85	2	6.13	133.81	5.65	1	2.14	40.38	
Q8IVM0	Coiled-coil domain-containing protein 50	CCDC50	12.09	4	5.93	246.02	22.55	7	6.94	218.74	
Q99985	Semaphorin-3C	SEMA3C	5.06	3	5.87	157.98	10.25	10	7.10	112.79	
Q9BW83	Intraflagellar transport protein 27 homolog	IFT27	28.49	3	5.63	191.31	4.30	1	3.49	35.20	
Q15293	Reticulocalbin-1	RCN1	33.53	8	5.62	710.33	16.92	6	6.00	189.21	
Q3V6T2	Girdin	CCDC88A	5.51	7	5.30	306.27	2.99	8	2.08	61.12	√
Q96S82	Ubiquitin-like protein 7	UBL7	11.05	3	4.97	217.39	5.00	2	2.22	41.60	
P12277	Creatine kinase B-type	CKB	57.74	14	4.90	2016.06	22.83	7	4.35	246.72	
Q49AR2	UPF0489 protein C5orf22	C5orf22	10.18	3	4.83	145.87	4.07	1	2.64	24.0	
P46940	IQ motif-containing GTPase-activating protein 1	IQGAP1	58.90	74	4.62	9207.69	22.09	35	2.94	844.81	√
P52292	Importin subunit alpha-2	KPNA2	31.76	13	4.45	1753.23	20.79	9	3.53	283.03	
Q92692	Poliovirus receptor-related protein 2	PVRL2	6.32	1	4.36	112.74	1.49	1	2.63	31.85	
P29317	Ephrin type-A receptor 2	EPHA2	18.24	12	4.32	574.42	1.33	1	4.82	18.0	√
P11717	Cation-independent mannose-6-phosphate receptor	IGF2R	10.52	18	4.30	1068.25	4.26	12	4.22	197.39	
Q8NBT2	Kinetochore protein Spc24	SPC24	20.30	2	4.30	100.81	15.74	4	2.04	30.85	
O15460	Prolyl 4-hydroxylase subunit alpha-2	P4HA2	13.64	5	3.92	275.68	15.89	8	2.59	150.06	
Q9H299	SH3 domain-binding glutamic acid-rich-like protein 3	SH3BGRL3	20.43	2	3.90	189.56	27.96	3	2.40	121.60	
Q02809	Procollagen-lysine,2-oxoglutarate 5-dioxygenase 1	PLOD1	37.55	18	3.89	2045.86	10.73	8	2.85	129.75	
P09972	Fructose-bisphosphate aldolase C	ALDOC	40.38	10	3.86	3091.05	37.64	14	2.08	784.90	
P49459	Ubiquitin-conjugating enzyme E2 A	UBE2A	17.76	2	3.85	116.66	6.58	1	2.74	52.84	
Q9BW71	HIRA-interacting protein 3	HIRIP3	3.06	1	3.74	70.67	1.44	1	2.05	38.00	
P12532	Creatine kinase U-type, mitochondrial	KCRU	11.27	3	3.67	184.95	13.19	5	2.13	181.47	
O14907	Tax1-binding protein 3	TAX1BP3	28.23	2	3.63	217.29	25.00	2	2.31	60.76	
Q5JTD0	Tight junction-associated protein 1	TJAP1	4.67	2	3.60	111.41	3.95	2	3.51	33.84	
Q96PU8	Protein quaking	QKI	18.48	4	3.60	322.96	14.08	3	2.52	81.22	
Q14008	Cytoskeleton-associated protein 5	CKAP5	24.36	42	3.39	2625.12	11.02	23	2.45	215.81	
Q9C0C2	182 kDa tankyrase-1-binding protein	TNKS1BP1	15.62	16	3.07	784.76	2.43	3	2.79	48.97	
Q96AY3	FK506 binding protein 10	FKBP10	21.82	8	3.06	437.31	18.56	10	2.72	291.52	
O00159	Unconventional myosin-Ic	MYO1C	36.78	26	3.03	2155.31	8.37	10	3.24	126.41	
O94992	Protein HEXIM1	HEXIM1	3.90	1	2.87	90.18	8.36	3	5.21	54.90	

TABLE I—*continued*

Accession number	Description	Symbol	Coverage (%)	Match peptides	H/L ratio	Mascot scores	Coverage (%)	Match peptides	116/114 ratio[a]	Mascot scores	Metastasis
Q02952	A-kinase anchor protein 12	AKAP12	18.97	17	2.86	1062.66	1.80	3	6.50	30.17	
Q15904	V-type proton ATPase subunit S1	ATP6AP1	11.28	4	2.85	186.77	7.87	4	3.29	23.72	
Q6PIU2	Neutral cholesterol ester hydrolase 1	NCEH1	15.69	4	2.84	473.80	11.27	4	2.85	102.16	
Q92890	Ubiquitin fusion degradation protein 1 homolog	UFD1L	32.57	7	2.83	411.96	21.50	7	2.41	100.81	
P51948	CDK-activating kinase assembly factor MAT1	MNAT1	16.18	2	2.81	147.19	8.41	4	2.05	105.44	
P30043	Flavin reductase (NADPH)	BLVRB	47.09	6	2.80	710.03	26.70	5	3.29	259.48	
Q96JB3	Hypermethylated in cancer 2 protein	HIC2	1.63	1	2.79	40.65	4.55	3	2.27	37.87	
P23368	NAD-dependent malic enzyme, mitochondrial	ME2	24.66	11	2.66	1012.54	12.50	8	4.44	170.95	
Q08J23	tRNA (cytosine(34)-C(5))-methyltransferase	NSUN2	37.29	16	2.60	1272.91	11.86	9	5.64	139.17	
P19525	Interferon-induced, double-stranded RNA-activated protein kinase	EIF2AK2	20.15	8	2.60	563.48	9.98	6	2.08	61.56	
O95400	CD2 antigen cytoplasmic tail-binding protein 2	CD2BP2	23.46	5	2.56	392.21	9.68	3	2.53	105.25	
P07355	Annexin A2	ANXA2	64.90	24	2.55	4096.69	53.69	21	5.19	1487.93	√
Q13242	Serine/arginine-rich splicing factor 9	SRSF9	21.27	5	2.54	234.06	16.29	4	2.06	58.81	
P17812	CTP synthase 1	CTPS1	24.70	12	2.52	1446.23	4.74	4	2.77	48.29	
O60664	Perilipin-3	PLIN3	63.82	17	2.52	3612.99	38.25	12	3.23	651.61	
Q96DG6	Carboxymethylenebutenolidase homolog	CMBL	13.88	2	2.49	112.51	13.06	4	2.49	98.89	
Q99439	Calponin-2	CNN2	45.95	9	2.42	1005.74	9.71	3	2.72	121.23	
Q6P1J9	Parafibromin	CDC73	14.69	6	2.40	694.53	9.79	5	2.39	195.85	
O75663	TIP41-like protein	TIPRL	37.50	5	2.38	394.65	12.50	4	2.01	55.03	
P04792	Heat shock protein beta-1	HSPB1	70.73	11	2.34	2172.83	48.29	11	28.54	1201.29	
P15311	Ezrin	EZR	31.91	19	2.28	3316.41	23.55	16	3.09	360.14	√
Q96JJ7	Thioredoxin-related transmembrane protein 3	TMX3	13.88	4	2.28	314.69	7.05	4	5.52	124.63	
Q9BUR4	Telomerase Cajal body protein 1	WRAP53	3.28	1	2.26	215.25	2.37	1	2.15	80.45	
Q14318	FK506-Binding Protein 8	FKBP8	19.17	5	2.24	710.68	7.77	2	2.68	95.14	
Q7LG56	Ribonucleoside-diphosphate reductase subunit M2 B	RRM2B	9.69	2	2.21	201.26	6.84	2	3.24	42.19	
O14828	Secretory carrier-associated membrane protein 3	SCAMP3	19.02	4	2.19	926.58	8.36	2	3.03	184.41	
O75410	Transforming acidic coiled-coil-containing protein 1	TACC1	7.95	4	2.15	442.71	1.61	2	2.51	22.36	
P04075	Fructose-bisphosphate aldolase A	ALDOA	68.68	19	2.14	6413.57	46.70	16	2.15	1366.74	
P43304	Glycerol-3-phosphate dehydrogenase, mitochondrial	GPD2	18.71	10	2.14	869.32	11.42	9	4.18	143.34	
P63313	Thymosin beta-10	TMSB10	31.82	1	2.12	192.50	61.36	3	2.39	224.01	
P26639	Threonine–tRNA ligase, cytoplasmic	TARS	37.07	19	2.11	1507.94	14.25	11	2.99	188.54	
Q16543	Hsp90 co-chaperone Cdc37	CDC37	27.25	10	2.08	1177.62	11.90	4	2.02	128.73	
P09493	Tropomyosin alpha-1 chain	TPM1	21.83	8	2.07	483.92	56.69	20	4.51	2085.88	
P51114	Fragile X mental retardation syndrome-related protein 1	FXR1	30.27	16	2.05	1027.50	13.20	10	2.17	152.74	
P36404	ADP-ribosylation factor-like protein 2	ARL2	32.07	4	2.03	458.43	14.13	3	4.09	66.74	
Q8WVJ2	NudC domain-containing protein 2	NUDCD2	22.29	2	2.02	382.36	6.37	1	2.38	21.0	

[a] 117/115 ratios are similar to 116/114 ratios. In this table, we only show the 116/114 ratios in iTRAQ experiment.

TABLE II
Down-regulated proteins (fold change < 0.5) in HuH-7^R cells

Accession number	Description	Symbol	Coverage (%)	Match peptides	H/L ratio	Mascot scores	Coverage (%)	Match peptides	116/114 ratio[a]	Mascot scores	Metastasis
Q15493	Regucalcin	RGN	5.69	1	0.034	144.88	15.72	4	0.096	81.07	
P35527	Keratin, type I cytoskeletal 9	KRT9	28.41	9	0.045	897.22	7.38	6	0.196	49.60	
Q96DC8	Enoyl-CoA hydratase domain-containing protein 3, mitochondrial	ECHDC3	13.86	2	0.071	129.67	8.25	2	0.195	36.11	
P28332	Alcohol dehydrogenase 6	ADH6	6.52	1	0.072	56.71	14.95	6	0.056	103.45	
P55809	Succinyl-CoA:3-ketoacid coenzyme A transferase 1, mitochondrial	OXCT1	11.92	3	0.081	99.65	6.92	3	0.282	53.14	
P55157	Microsomal triglyceride transfer protein large subunit	MTTP	26.06	16	0.101	684.92	25.62	20	0.103	527.12	
Q13423	NAD(P) transhydrogenase, mitochondrial	NNT	15.10	10	0.104	916.85	10.77	11	0.138	277.28	
P48728	Aminomethyltransferase, mitochondrial	AMT	3.47	1	0.111	91.44	1.99	1	0.109	22.01	
P21397	Amine oxidase [flavin-containing] A	MAOA	11.20	4	0.115	181.98	9.11	6	0.093	73.67	
P32189	Glycerol kinase	GK	20.21	9	0.129	550.13	15.56	9	0.165	84.68	
P23141	Liver carboxylesterase 1	CES1	53.44	24	0.152	5133.25	24.34	12	0.169	622.79	
Q13228	Selenium-binding protein 1	SELENBP1	2.75	1	0.153	48.25	11.02	4	0.127	154.39	
P00352	Retinal dehydrogenase 1	ALDH1A1	60.68	25	0.159	6964.85	31.14	14	0.318	253.37	
P15144	Aminopeptidase N	ANPEP	2.17	2	0.160	75.51	10.13	10	0.235	190.45	
P00367	Glutamate dehydrogenase 1, mitochondrial	GLUD1	39.43	17	0.164	2869.48	35.48	20	0.064	1497.60	
Q96CM8	Acyl-CoA synthetase family member 2, mitochondrial	ACSF2	8.62	3	0.168	297.04	6.34	4	0.417	36.70	
P00966	Argininosuccinate synthase	ASS1	31.80	7	0.168	262.42	4.85	3	0.276	23.84	
Q86TX2	Acyl-coenzyme A thioesterase 1	ACOT1	40.38	10	0.170	874.14	15.91	7	0.297	188.53	
O43175	D-3-phosphoglycerate dehydrogenase	PHGDH	49.72	17	0.171	1551.32	18.57	9	0.126	432.92	
P11498	Pyruvate carboxylase, mitochondrial	PC	35.40	25	0.172	3147.43	15.11	14	0.068	220.94	
P42330	Aldo-keto reductase family 1 member C3	AKR1C3	57.28	14	0.174	4764.61	21.05	9	0.046	332.48	
O60701	UDP-glucose 6-dehydrogenase	UGDH	60.93	23	0.183	4150.41	15.99	7	0.133	153.19	
P49888	Estrogen sulfotransferase	SULT1E1	7.14	1	0.185	45.56	5.44	2	0.209	81.80	
P05091	Aldehyde dehydrogenase, mitochondrial	ALDH2	26.11	10	0.191	997.67	31.72	15	0.204	565.98	
P32119	Peroxiredoxin-2	PRDX2	35.86	7	0.203	661.98	33.33	8	0.149	453.16	
Q02252	Methylmalonate-semialdehyde dehydrogenase [acylating], mitochondrial	ALDH6A1	19.44	8	0.205	260.38	23.36	10	0.303	219.25	
Q9H3G5	Probable serine carboxypeptidase CPVL	CPVL	13.24	5	0.211	319.41	4.20	3	0.272	45.97	
P50225	Sulfotransferase 1A1	SULT1A1	28.81	5	0.218	439.29	20.34	8	0.144	37.04	
O75874	Isocitrate dehydrogenase [NADP] cytoplasmic	IDH1	45.17	14	0.220	2770.34	33.57	14	0.257	598.48	
Q9Y365	PCTP-like protein	STARD10	10.31	2	0.220	215.94	9.62	2	0.092	48.96	
Q96C23	Aldose 1-epimerase	GALM	19.59	4	0.221	347.19	14.04	4	0.089	181.34	
Q9ULC5	Long-chain-fatty-acid–CoA ligase 5	ACSL5	26.94	13	0.225	1026.06	18.89	13	0.049	263.76	
P78330	Phosphoserine phosphatase	PSPH	32.44	5	0.233	537.24	25.33	5	0.215	191.88	
P45954	Short/branched chain specific acyl-CoA dehydrogenase, mitochondrial	ACADSB	19.91	5	0.236	489.46	23.61	8	0.242	146.90	
P16401	Histone H1.5	HIST1H1B	10.18	3	0.238	119.03	31.86	9	0.245	675.56	
Q6P587	Acylpyruvase FAHD1, mitochondrial	FAHD1	33.48	4	0.250	322.07	3.57	1	0.446	31.41	
Q08426	Peroxisomal bifunctional enzyme	EHHADH	7.19	4	0.260	185.39	15.35	11	0.031	264.25	
P09455	Retinol-binding protein 1	RBP1	32.59	4	0.260	216.97	24.44	3	0.366	177.82	
P23378	Glycine dehydrogenase [decarboxylating], mitochondrial	GLDC	15.49	10	0.261	696.72	7.06	7	0.013	149.08	
P56199	Integrin alpha-1	ITGA1	4.58	4	0.272	131.10	4.92	8	0.429	28.65	
Q00796	Sorbitol dehydrogenase	SORD	34.73	8	0.291	1004.66	21.85	6	0.403	101.08	

TABLE II—*continued*

Accession number	Description	Symbol	Coverage (%)	Match peptides	H/L ratio	Mascot scores	Coverage (%)	Match peptides	116/114 ratio[a]	Mascot scores	Metastasis
Q9Y617	Phosphoserine aminotransferase	PSAT1	30.27	9	0.292	935.75	29.73	12	0.127	224.59	
P51812	Ribosomal protein S6 kinase alpha-3	RPS6KA3	31.22	18	0.312	1508.24	21.22	17	0.089	407.58	
Q08623	Pseudouridine-5′-monophosphatase	HDHD1	12.28	3	0.315	260.60	8.33	2	0.489	31.00	
P13804	Electron transfer flavoprotein subunit alpha, mitochondrial	ETFA	50.15	10	0.320	1796.72	25.23	6	0.369	149.78	
P15374	Ubiquitin carboxyl-terminal hydrolase isozyme L3	UCHL3	31.30	5	0.323	603.32	19.57	4	0.293	68.79	
P30405	Peptidyl-prolyl cis-trans isomerase F, mitochondrial	PPIF	27.05	2	0.329	366.13	17.39	5	0.243	85.43	
Q2PPJ7	Ral GTPase-activating protein subunit alpha-2	RALGAPA2	2.35	3	0.336	122.83	1.71	4	0.044	58.45	√
Q9P015	39S ribosomal protein L15, mitochondrial	MRPL15	16.89	3	0.338	379.63	15.20	5	0.407	42.49	
Q5T6V5	UPF0553 protein C9orf64	C9orf64	26.69	7	0.348	623.85	12.61	4	0.220	64.10	
P38117	Electron transfer flavoprotein subunit beta	ETFB	45.49	12	0.359	1048.97	43.53	12	0.281	250.59	
Q9NRF8	CTP synthase 2	CTPS2	19.45	8	0.364	819.80	8.53	5	0.017	43.45	
Q15125	3-beta-hydroxysteroid-Delta(8), Delta(7)-isomerase	EBP	6.96	1	0.365	106.53	11.30	2	0.371	38.10	
Q9UIJ7	GTP:AMP phosphotransferase, mitochondrial	AK3	20.70	3	0.368	496.73	32.16	7	0.446	123.54	
O15228	Dihydroxyacetone phosphate acyltransferase	GNPAT	13.68	7	0.379	533.17	4.41	3	0.282	38.20	
P35754	Glutaredoxin-1	GLRX	23.58	3	0.388	190.41	10.38	1	0.097	35.60	
P48506	Glutamate–cysteine ligase catalytic subunit	GCLC	7.69	5	0.390	369.81	4.55	3	0.394	55.76	
Q9HC35	Echinoderm microtubule-associated protein-like 4	EML4	12.23	9	0.404	667.70	10.70	10	0.229	198.44	
O14936	Peripheral plasma membrane protein CASK	CASK	7.02	4	0.407	369.08	7.13	9	0.350	39.70	
P51690	Arylsulfatase E	ARSE	8.49	3	0.407	185.17	7.64	4	0.253	111.16	
P09417	Dihydropteridine reductase	QDPR	43.85	6	0.411	705.23	31.97	5	0.377	130.89	
P11766	Alcohol dehydrogenase class-3	ADH5	34.49	7	0.422	846.22	11.23	5	0.353	128.03	
P21291	Cysteine and glycine-rich protein 1	CSRP1	19.17	2	0.423	111.06	11.92	2	0.430	58.02	
O94832	Unconventional myosin-Id	MYO1D	2.49	2	0.423	125.92	6.06	8	0.416	55.25	
Q9BRX8	Redox-regulatory protein FAM213A	FAM213A	16.59	3	0.432	292.31	26.64	6	0.294	144.68	
Q9NQ94	APOBEC1 complementation factor	A1CF	8.92	4	0.442	316.45	6.06	4	0.373	29.11	
P28288	ATP-binding cassette sub-family D member 3	ABCD3	21.70	12	0.447	1180.54	6.07	4	0.196	78.63	
P25325	3-mercaptopyruvate sulfurtransferase	MPST	22.90	4	0.447	521.80	19.53	5	0.365	107.95	
Q13126	S-methyl-5′-thioadenosine phosphorylase	MTAP	25.09	4	0.448	520.92	6.01	2	0.371	36.03	
Q14571	Inositol 1,4,5-trisphosphate receptor type 2	ITPR2	1.37	4	0.456	187.79	4.85	14	0.490	68.61	
Q9H0U6	39S ribosomal protein L18, mitochondrial	MRPL18	5.00	1	0.457	50.52	7.22	1	0.459	48.78	
P27144	Adenylate kinase isoenzyme 4, mitochondrial	AK4	11.66	2	0.464	361.78	24.22	5	0.144	73.66	
Q9BRF8	Calcineurin-like phosphoesterase domain-containing protein 1	CPPED1	12.42	3	0.478	274.46	6.37	2	0.177	86.52	
Q8NBQ5	Estradiol 17-beta-dehydrogenase 11	HSD17B11	23.67	5	0.486	371.70	15.00	5	0.420	148.64	
O94905	Erlin-2	ERLIN2	27.73	8	0.492	823.15	34.51	10	0.480	246.01	

[a] 117/115 ratios are similar to 116/114 ratios. In this table, we only show the 116/114 ratios in iTRAQ experiment.

TABLE III
The top three biological networks in the dual quantitative proteomics based on IPA

Network ID	Top functions of up-regulated proteins	Score	Focus molecules	Molecules in network
1	Cellular Movement, Cell-To-Cell Signaling and Interaction, Tissue Development	47	24	**AKAP12**, AKT, **ANXA1**, **ANXA2**, **CCDC88A**, **CDC37**, **CTGF**, **EIF2AK2**, ERK, ERK1/2, estrogen receptor, **EZR**, **FKBP8**, FSH, **HEXIM1**, Hsp90, **HSPB1**, **IGF2R**, IgG, **IQGAP1**, **ISG15**, Jnk, **LDLR**, **LGALS1**, Lh, **MVP**, **MYO1C**, NFkB (complex), **OPTN**, P38 MAPK, **P4HA2**, **PLIN3**, **SDCBP**, **SRSF9**, **VIM**
2	Cell Death and Survival, Cell Cycle, Cancer	20	13	CCNA2, **CDC37**, **CKAP5**, CSE1L, CTCF, DYNLL1, E4F1, ESR1, FKBP4, glutathione peroxidase, HLA-DQA1, KIF24, **KPNA2**, LTBP1, MAPK12, **ME2**, **MNAT1**, PAX6, **PFKM**, **PFKP**, PRDM5, **RRM2B**, S100A2, **TACC1**, TMEM97, **TMSB10/TMSB4X**, TOP2B, TP53, TP53AIP1, TP53I3, **UBL7**, **VIM**, **WRAP53**
3	Cancer, Endocrine System Disorders, Cardiac Hypertrophy	18	12	**ABCF2**, ADCY9, AGTR1, **ALDOA**, **ALDOC**, **ATP6AP1**, CHKA, **CKB**, CORO1A, **CTPS1**, EGFR, EPAS1, **EPHA2**, FAM13A, HIF1A, HLA-DRB3, **LDHB**, MB, **NSUN2**, NUCKS1, **NUDCD2**, NUPR1, RAB11FIP5, RPN2, **SCAMP3**, SLC6A6, **SPC24**, SYVN1, TAF9B, **TARS**, TMEM19, TMEM45A, TMPRSS6, TRERF1, ZPR1
Network ID	Top functions of down-regulated proteins	Score	Focus molecules	Molecules in network
1	Drug Metabolism, Endocrine System Development and Function	25	14	**AK4**, **AKR1C3**, AKR1C4, **ALDH1A**, **ANPEP**, CREBL2, CTNNB1, **EBP**, **ECHDC3**, **EML4**, F11, FABP1, **FAM213A**, FUK, FUT3, FUT5, FUT6, FUT10, FUT11, GMDS, GOT1, **HDHD1**, HNF1A, HNF4A, HSD17B2, **HSD17B11**, **ITGA1**, **MTTP**, PGR, **PPIF**, SERPINA5, SUZ12, **UCHL3**, UGT1A9,
2	Amino Acid Metabolism, Small Molecule Biochemistry	22	13	ABCC5, **ABCD3**, ADORA1, **ALDH2**, **ASS1**, ATF4, **CASK**, **CSRP1**, ESR1, FANCC, FBXO31, **GCLC**, GPR176, GRM1, HAMP, IL17RB, KDELR3, MKK3/6, P38 MAPK, **PHGDH**, PIK3R3, **PRDX2**, PRSS23, **PSAT1**, **PSPH**, **RBP1**, **RPS6KA3**, Sod, **SORD**, TCR, TM4SF1, TNF, TNFAIP6, TRIM27, UXT
3	Development Disorder, Organism Injury and Abnormalities	20	12	**ACSL5**, **ADH5**, ALOX15B, ALX1, ANK1, AR, ARHGAP11A, CCNF, CDH1, **CPVL**, **CTPS2**, DEPTOR, DSE, **GK**, **GLRX**, **HIST1H1B**, HNRNPA2B1, **IDH1**, **ITPR2**, MAGI1, **MAOA**, MAPK1, MX2, NUPR1, PLK3, PTGER3, RELA, SAMHD1, SLC2A12, SLC39A8, SP1, **SULT1A1**, TMEM158, TNS3, **UGDH**

TABLE IV
Up-regulated (fold change > 2.0) and quantified proteins in HuH-7^R cells analyzed by IPA

Level changed molecules (n = 81)		
Functions & Diseases	p value	Molecules
Metastasis	3.79E-08	AKAP12, AKT, ANXA1, CCDC88A, CTGF, EPHA2, EZR, FKBP8, HEXIM1, LGALS1, NFkB, SDCBP, VIM
Formation of cellular protrusions	7.91E-07	AKAP12, AKT, CCDC88A, CTGF, EPHA2, ERK1/2, EZR, FSH, HSPB1, IQGAP1, NFkB, OPTN, P38 MAPK, VIM
Liver cancer	9.88E-05	ANXA1, ANXA2, EIF2AK2, estrogen receptor, Hsp90, IGF2R, IQGAP1, ISG15, NFkB, VIM
Proliferation of tumor cells	1.66E-03	AKT, ANXA1, ANXA2, CTGF, EPHA2, ERK1/2, estrogen receptor, EZR, FKBP8, Hsp90, IQGAP1, Jnk, LGALS1, NFkB
Quantified molecules (n = 1,822)		
Canonical Pathway	p value	
mTOR Signaling	1.12E-21	
PI3K/AKT Signaling	3.56E-05	

value close to that for HuH-7 cells. Taken together, these results show that knockdown of galectin-1 not only attenuates cell proliferation and metastasis in HuH-7^R cells, it also restores sorafenib sensitivity.

High Expression of Galectin-1 in HuH-7^R Cells Promotes Tumorigensis and Pulmonary Metastasis In Vivo—To further assess the tumorigenic and metastatic potential of HuH-7^R cells, which express galectin-1 at elevated levels, we employed mouse xenograft tumor models created by subcutaneous or tail vein injection of HuH-7 or HuH-7^R cells. As shown in Fig. 5*A*, HuH-7^R cells exhibited enhanced tumorigenic ability compared with HuH-7 cells. Immunohistochem-

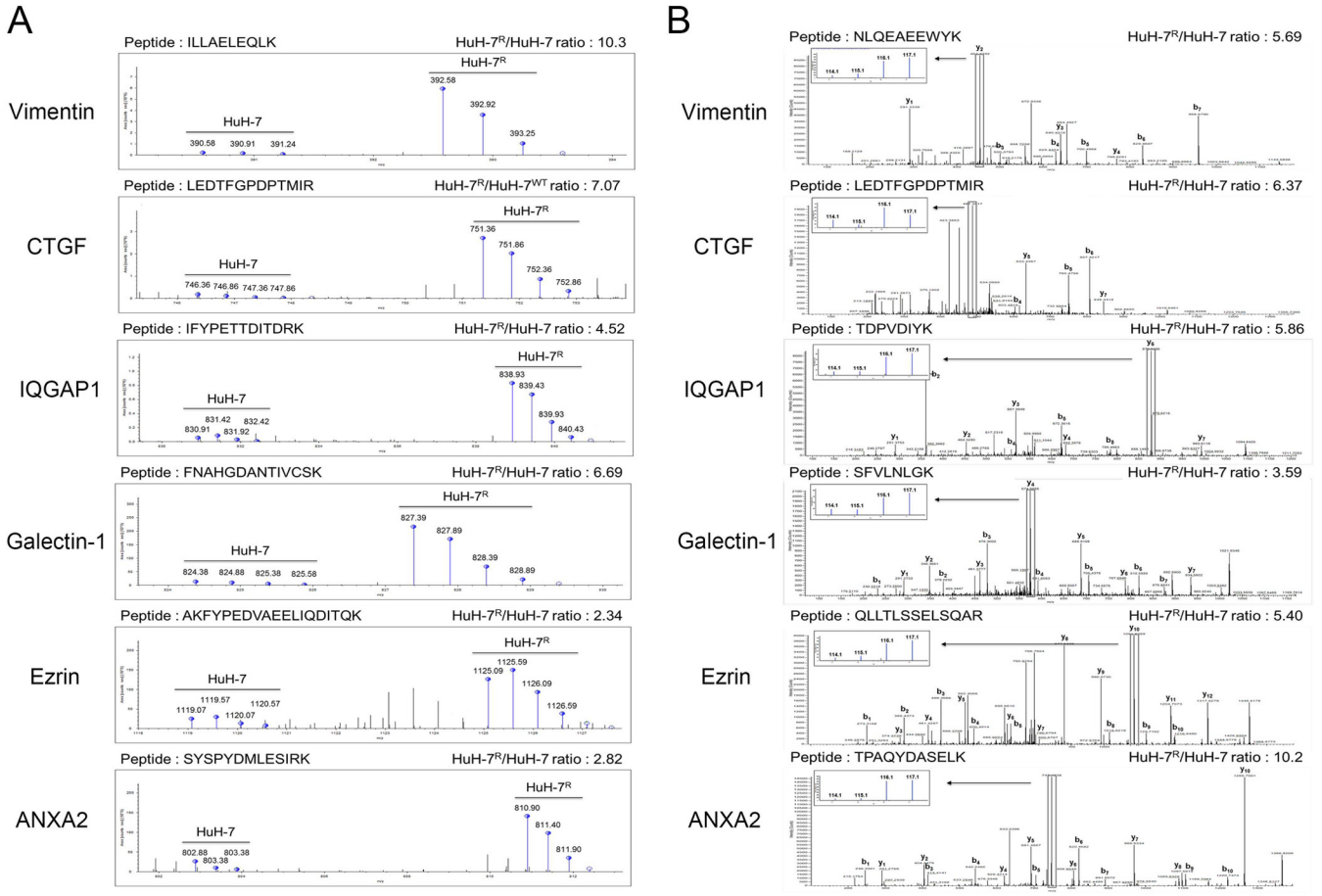

FIG. 3. **Selected EMT-related candidates identified by quantitative MS.** *A*, SILAC spectra are shown for sorafenib-regulated proteins. *B*, iTRAQ spectra are shown for sorafenib-regulated proteins. MS spectrum, identified peptide sequence, and quantified HuH-7^R/HuH-7 ratio are presented. CTGF, connective tissue growth factor; IQGAP1, IQ motif-containing GTPase-activating protein 1; ANXA2, annexin A2.

istry revealed intense staining for galectin-1 and the proliferation marker Ki-67 in tumors formed by HuH-7^R cells, showing that proliferation rates were increased in these galectin-1-overexpressing tumors (Fig. 5*B*). Moreover, elevated galectin-1 expression in HuH-7^R cells might correlate with the enhanced development of pulmonary metastatic nodules (Fig. 5*C* and 5*D*). Taken together, these results suggest that HuH-7^R cells have greater tumorigenic and metastatic potential than HuH-7 cells *in vivo*.

Galectin-1 Expression is Regulated by PI3K/AKT, mTOR, and HIF-1α Pathways—Bioinformatics analyses indicated that up-regulation of the mTOR (mammalian target of rapamycin) signaling pathway could be involved in facilitating the sorafenib resistance of HuH-7^R cells (Table IV). To test this, we examined the involvement of the mTOR-signaling pathway in galectin-1 expression in HuH-7^R cells. Time-course experiments showed that treatment of HuH-7^R cells with rapamycin (an inhibitor of mTOR) almost completely blocked phosphorylation of eukaryotic translation initiation factor 4E binding protein 1 (4EBP1), ribosomal protein S6 kinase, 70 kDa (P70S6K) and ribosomal protein S6 (S6), and markedly attenuated expression of galectin-1 at the protein level (Fig. 6*A*). Furthermore, we found that inhibition of AKT phosphorylation with the phosphoinositide 3-kinase (PI3K) inhibitor LY294002 significantly reduced galectin-1 expression in HuH-7^R cells (Fig. 6*B*). Moreover, we also detected the mRNA level of galectin-1 declined after LY294002 and rapamycin treatment, respectively (Fig. 6*D*, upper panel). These data suggest that both the AKT and mTOR pathways are involved in galectin-1 up-regulation.

A previous study showed that galectin-1 is a direct target of the transcription factor, hypoxia inducible factor 1 alpha (HIF-1α) (11). To explore further the linkage between HIF-1α and galectin-1 in HuH-7^R cells, we exposed the cells to the well-known hypoxia-mimetic agent, $CoCl_2$. $CoCl_2$ significantly enhanced galectin-1 protein expression in a time-dependent manner (Fig. 6C), and also increased galectin-1 mRNA levels (Fig. 6*D*, upper panel). To further confirm that these effects are mediated by transcriptional activation of the galectin-1 gene, we examined binding of HIF-1α to the endogenous *galectin-1* promoter in HuH-7^R cells, with or without $CoCl_2$ treatment, using ChIP assays. In the chromatin fraction pulled down by

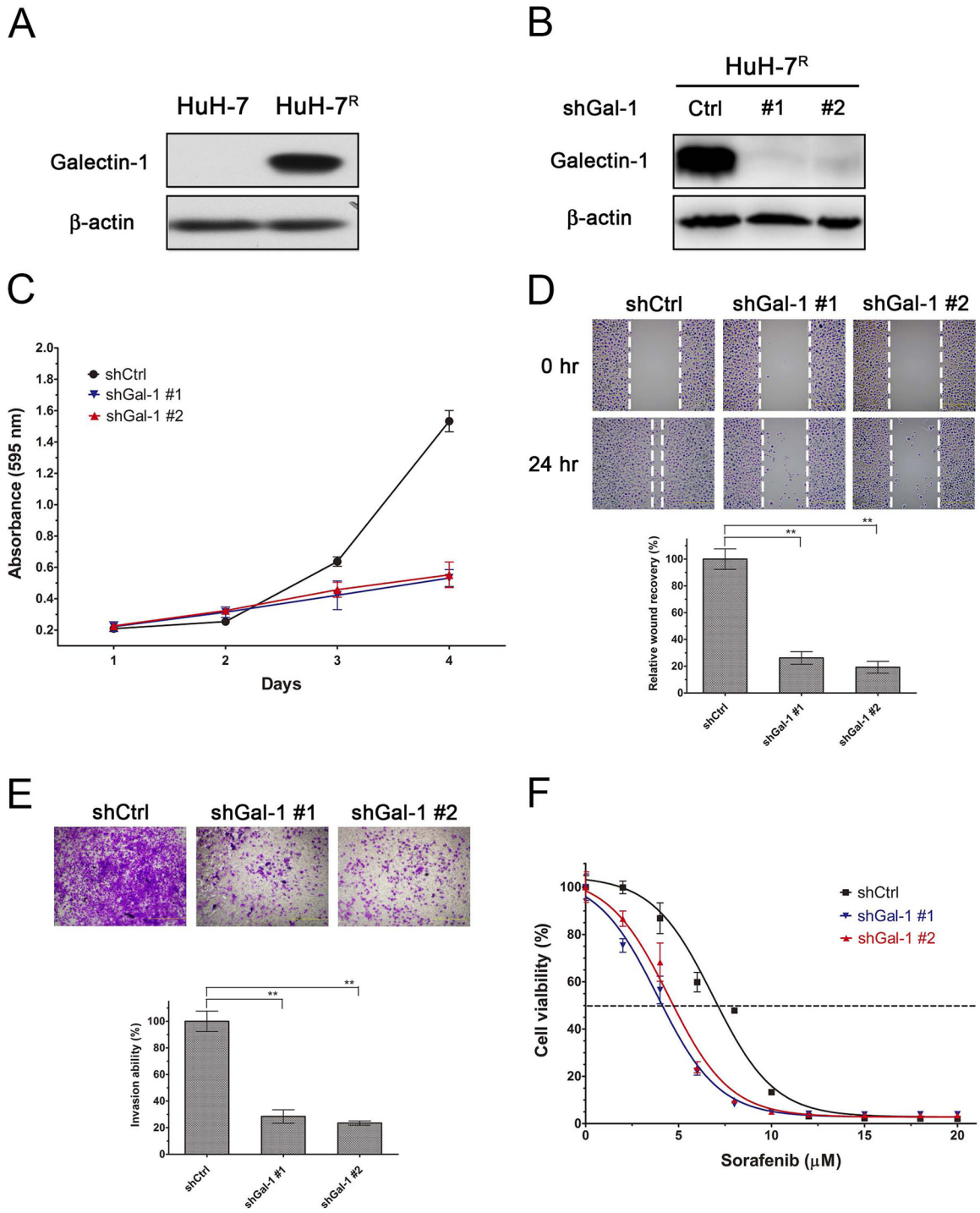

FIG. 4. **Galectin-1 contributes to proliferation, migration, invasion, and sorafenib sensitivity.** *A*, The expression level of Gal-1 in HuH-7 and HuH-7^R cells determined by immunoblotting analysis. *B*, HuH-7^R cells were transfected with shGal-1 (#1, #2) or control shRNA (shCtrl), and 72 h later the cells were lysed and analyzed by immunoblotting with the indicated antibodies. *C*, Viability of shGal-1-knockdown HuH-7^R cells was determined at the indicated time points by MTT assay. Plots show cumulative cell numbers *versus* days in culture. *D*, Wound-healing assays of shGal-1-knockdown HuH-7^R cells. The micrographs show cells that had migrated into the gap 0 h and 24 h after removal of the insert. *E*, Transwell migration assays of shGal-1-knockdown HuH-7^R cells. Cells in the central field of each insert were visualized by light microscopy and quantified. *F*, shGal-1-knockdown cells were exposed to sorafenib at the indicated concentrations for 72 h, and cell viability was analyzed by MTT assay. The concentration-response curve for sorafenib in the shGal-1-knockdown group was shifted toward a lower concentration compare with that for shCtrl HuH-7^R cells. Data are presented as means ± S.D., and are representative of at least three independent biological replicates. shGal-1, shRNA against galectin-1; shCtrl, control shRNA.

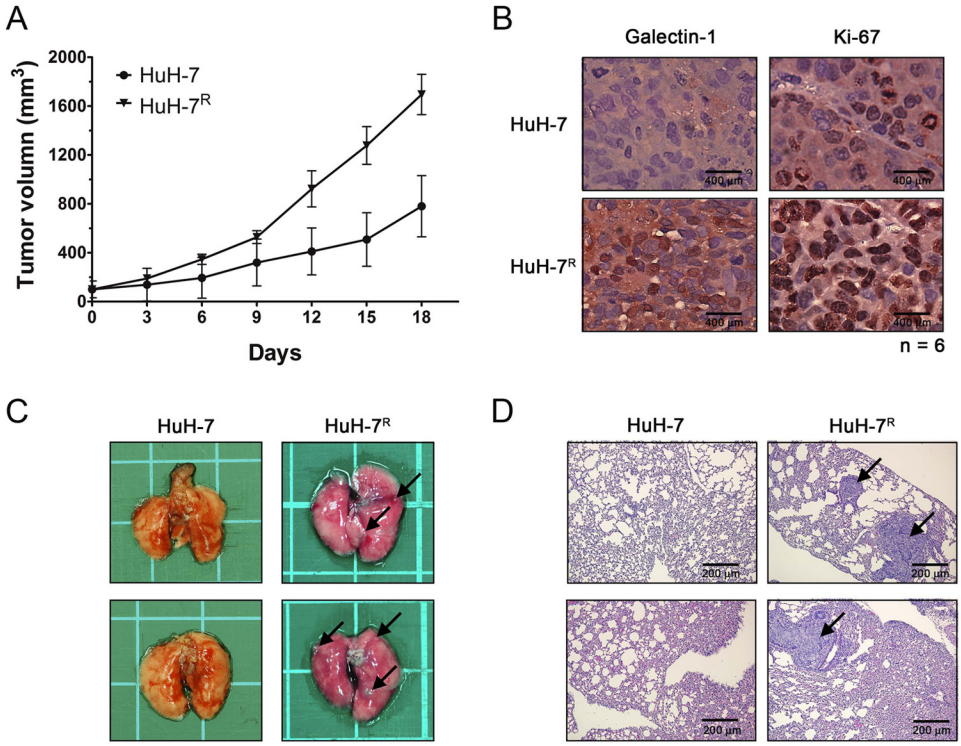

FIG. 5. **High expression of galectin-1 in HuH-7^R cells promotes tumorigensis and pulmonary metastasis in an animal model.** *A*, Nude mice were injected subcutaneously with HuH-7 or HuH-7^R cells. Tumor volume at the indicated time points was calculated and plotted (n = 6/group). *B*, Representative images (x40) of xenograft tissue showing immunohistochemistry staining for galectin-1 and Ki-67. *C*, Gross appearance of two representative lungs from each group of mice. The length of the small-scale bar corresponds to 1 cm. Tumor nodules are indicated by arrows. *D*, Two representative images of H&E stained lungs from mice in each group. The scale bars shown on 5× images correspond to 1 mm. Tumor nodules are indicated by arrows.

an anti-HIF-1α antibody, *galectin-1* promoter PCR fragments were more abundant in $CoCl_2$-treated cells than in control cells (Fig. 6*D*, lower panel). Taken together, these results show that the expression of galectin-1 is mediated by the PI3K/AKT/mTOR/HIF-1α pathway (Fig. 6*E*).

Prognostic Value of Galectin-1 in Advanced HCC Patients—To determine whether galectin-1 expression is predictive of sorafenib resistance, we examined baseline galectin-1 levels before sorafenib treatment in 91 advanced HCC patients using ELISA. The basic characteristics of the 91 advanced HCC patients were showed in Supplemental Table S3. As shown in Fig. 7*A*, the mean ± S.D. level of serum galectin-1 from 17 healthy volunteers was 89.9 ± 30.2 ng/ml (range: 49.8–148.5 ng/ml). Using the maximum value of serum galectin-1 for healthy volunteers as the cutoff point, we found that patients with high pretreatment galectin-1 levels (i.e. >148.5 ng/ml) had significantly lower disease control rates (48%) than patients with low pretreatment galectin-1 levels (72%, $p = 0.023$; supplemental Table S4). Response rates in patients with high galectin-1 levels also trended lower compared with patients with low galectin-1 levels (2% *versus* 10%), although this difference did not reach statistical significance. Compared with patients with low galectin-1 levels, patients with high pretreatment galectin-1 levels also had significantly shorter median progression-free survival (2.2 *versus* 4.2 months, $p = 0.026$; Fig. 7*B*) and overall survival (6.1 *versus* 10.7 months, $p = 0.050$; Fig. 7*C*). After adjusting for other potential prognostic factors, multivariate analyses showed that high pretreatment galectin-1 levels remained an independent predictor of shorter progression-free survival (HR = 1.888, $p = 0.008$) and overall survival (HR = 2.179, $p = 0.002$) (supplemental Table S5). Notably, an examination of 29 HCC patients who developed progressive disease after sorafenib treatment showed a dramatic increase in serum galectin-1 concentration (Fig. 7*D*). Our data thus indicate that high galectin-1 serum level is associated with poor treatment efficacy of sorafenib, and shorter survivals in advanced HCC patients treated with sorafenib.

DISCUSSION

Sorafenib is a kinase-targeted drug for treatment of advanced HCC, but its use is hampered by the development of drug resistance. Therefore, understanding the molecular changes that underlie the biological consequences of acquired drug resistance is of critical importance. In this study, we performed dual SILAC and iTRAQ quantitative proteomics, allowing a broad, systematic examination of changes in the proteome that are associated with the acquisition of sorafenib

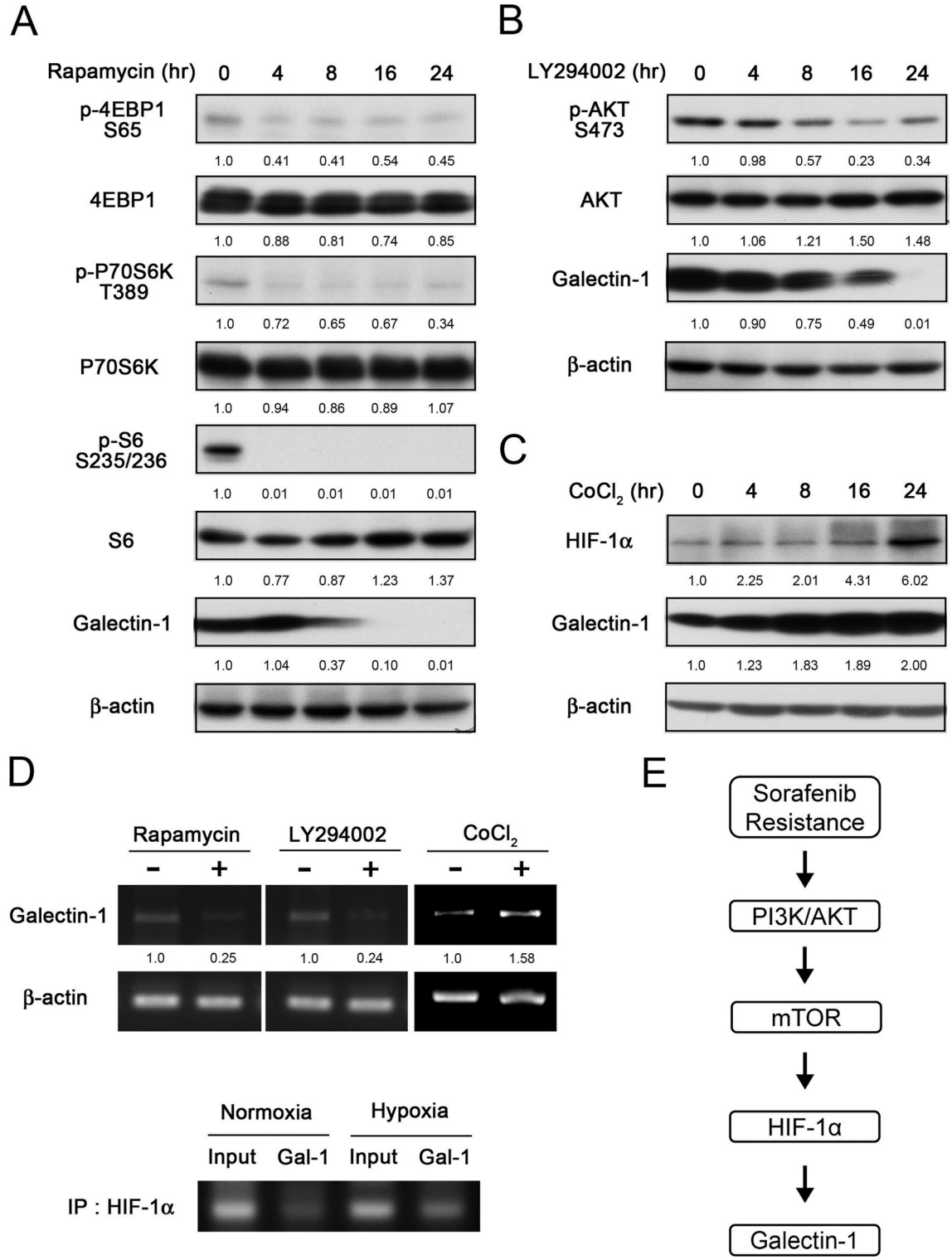

FIG. 6. **Galectin-1 is a downstream target of the AKT/mTOR-HIF1α signaling pathway in HuH-7^R cells.** HuH-7^R cells were treated with the inhibitors rapamycin (100 nM) *A*, LY294002 (10 μM) *B*, or $CoCl_2$ (150 μM) *C*, for the indicated times, after which HuH-7^R cell lysates were prepared and analyzed by immunoblotting with the indicated antibodies. At least three independent biological replicates of each study were performed. *D*, Upper panel: galectin-1 expression was analyzed by RT-PCR in HuH-7^R cells treated with inhibitors rapamycin (100 nM), LY294002 (10 μM) for 8 h and 150 μM $CoCl_2$ for 24 h; β-actin was used as a control. Lower panel: HuH-7^R cells were grown under normoxia or hypoxia ($CoCl_2$), after which ChIP assays were performed. *E*, Schematic illustration of galectin-1 expression mediated by the AKT/mTOR/HIF-1α signaling pathway in HuH-7 ^{R} cells.

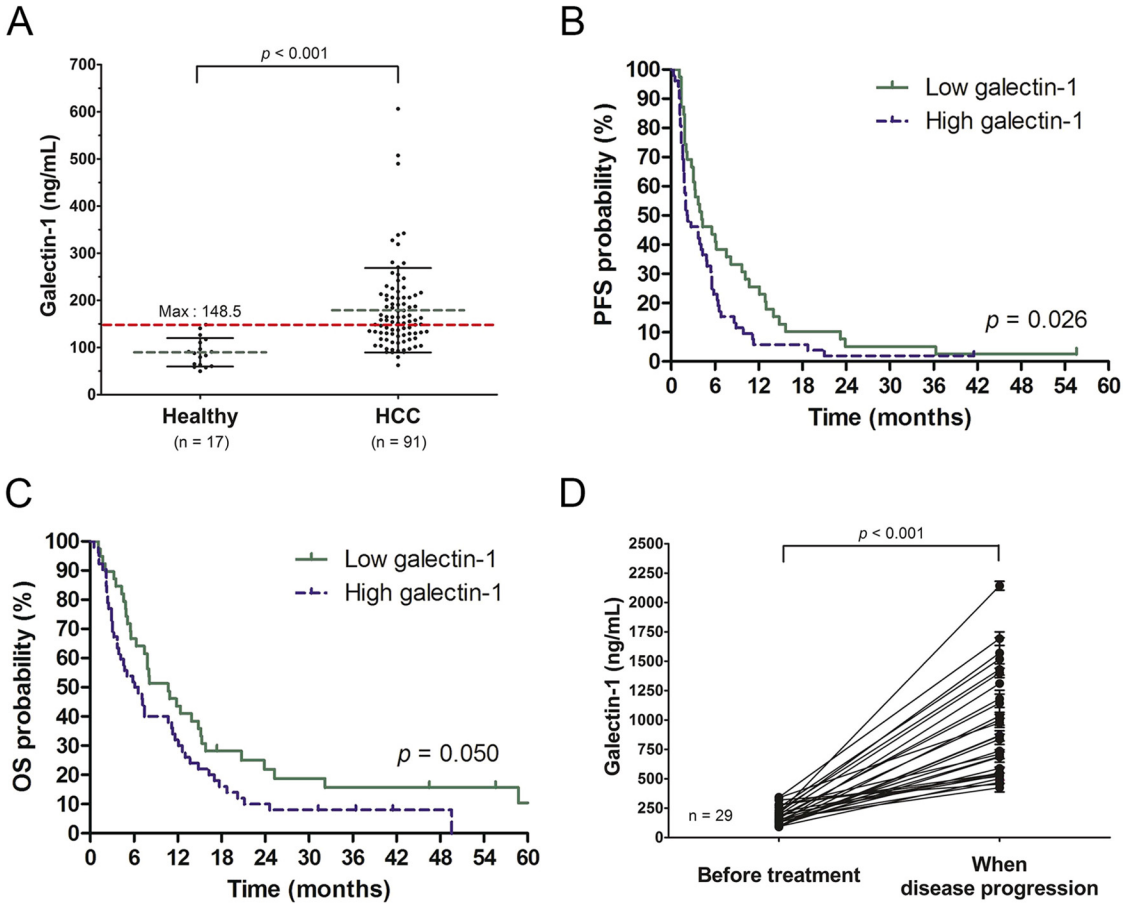

FIG. 7. **Galectin-1 is highly expressed in HCC serum samples and HCC patients treated with sorafenib.** *A*, Serum levels of galectin-1 in healthy volunteers ($n = 17$; mean = 89.9 ng/ml) and patients with advanced HCC ($n = 91$; mean = 179.6 ng/ml). Patients with advanced HCC had significantly higher serum galectin-1 levels than healthy volunteers ($p < 0.001$). The horizontal lines indicate means ± S.D. *B* and *C*, Kaplan-Meier analysis of progress-free survival *B*, and overall survival *C*, of patients with advanced HCC, grouped according to high and low pretreatment galectin-1 levels. *p* values are based on log-rank tests. *D*, Serum galectin-1 levels in patients before sorafenib treatment and upon disease progression during sorafenib treatment ($n = 29$). Serum galectin-1 levels significantly increased with disease progression ($p < 0.001$). PFS, progress-free survival; OS, overall survival.

resistance. The 156 differentially expressed proteins revealed a distinct signaling and EMT protein signature associated with sorafenib resistance in HuH-7^R cells. Among these proteins, 10 were linked to cellular movement, growth/proliferation, and cancer. Notably, our data showed that galectin-1 was linked to the AKT/mTOR/HIF-1α pathway, supporting galectin-1 as a predictive biomarker for sorafenib resistance.

As previous reports indicated, when 400 mg of sorafenib was given twice daily, the concentration of sorafenib in human plasma was between 5 and 7 mg/L, which is 7.8–10.9 μM in humans (15). In order to investigate the molecular mechanism of the acquired resistance to sorafenib, we developed HuH-7^R cells, which in the clinically relevant dose about 10 μM (the highest clinical achievable concentration). We showed that long-term exposure to sorafenib of HuH-7 cells changed their morphology into spindle shaped cells. These features are typical seen in cells undergoing EMT(16). Moreover, EMT is observed in HuH-7^R cells for loss of E-cadherin and gain of vimentin by Western blotting (Supplemental Fig. S6). The sorafenib resistant cells showed an activation of the EMT process with enhanced invasive and metastatic potentials. We also performed wound-healing and invasion assays, which revealed that migration rate and invasiveness were significantly up-regulated in HuH-7^R cells compared with HuH-7 cells. Recent reports have indicated that the emergence of drug resistance may link EMT as a contributing mechanism, such as cisplatin resistance in ovarian cancer (17) and gefitinib resistance in lung cancer (18). Therefore, this indicated that the selected cells should mimic the tolerance of sorafenib and behavior as the HCC in drug resistance patients.

Among the 10 differentially expressed proteins were associated with cell motility or invasion (19–28), nine were significantly increased in the highly metastatic HuH-7^R cells compared with the poorly metastatic HuH-7 cells, whereas one was notably decreased. Consistent with the possible metastasis-related functions of vimentin and ezrin, considerable evidence have shown that both proteins are responsible for

maintaining cell shape, stabilizing cytoskeletal interactions and cell motility (20, 25). Furthermore, annexin A1 is a key regulator of pathological angiogenesis and physiological angiogenic balance (29). Attenuated expression of RALGAPA2 leads to tumor invasion and metastasis of bladder cancer (21). Gridin regulates reorganization of the actin cytoskeleton and modulation of AKT activity, which ultimately result in cancer invasion and angiogenesis (30). Annexin A2, IQGAP1, and EPHA2 are closely associated with drug resistance. Annexin A2 involved in cell adhesion, cell motility, and expressed at higher levels in metastatic cancer and is associated with a drug-resistant phenotype. IQGAP1, which regulates cellular activities associated with cell–cell adhesion and cell migration, is overexpressed in trastuzumab-resistant breast epithelial cells; reducing IQGAP1 both increases the inhibitory effects of trastuzumab and restores trastuzumab sensitivity (31). EPHA2 belongs to the ephrin receptor subfamily of the protein-tyrosine kinase family. Cancer cells that overexpress EPHA2 exhibit increased motility and invasive properties, consistent with a prometastatic phenotype. Consistent with this, silencing EPHA2 inhibits proliferation and invasion, and increases sensitivity to paclitaxel (32). CTGF and galectin-1 are secreted proteins that are important in tumor growth, angiogenesis, and metastasis. CTGF modulates the invasion of certain human cancer cells through binding to integrins (19). Dysregulation of galectin-1 in cancer has also been correlated with the aggressiveness of tumors (33). Taken together, these observations suggest that metastasis is one of the most important causes of poor prognosis in patients with HCC. We hypothesize that the above proteins are involved in adverse responses to sorafenib, although additional study will be needed to verify their specific roles in sorafenib resistance.

The goal of our study was to investigate the potential use of proteins that are differentially released from HCC cells as predictive or prognostic biomarkers for HCC patients treated with sorafenib. Biomarker for predicting the efficacy of sorafenib is a growing field and a number of candidate markers have been proposed. Low HGF levels and high c-kit levels in plasma at baseline were reported to be associated with longer survival in HCC patients treated with sorafenib (9). Several serum angiogenesis-related cytokines levels were correlated with response to sorafenib treatment (9, 34). Some tissue markers, such as $\alpha\beta$-crystallin (35), FGF3/FGF4 (36), JNK (37), and pERK (38) have been reported to predict sorafenib response. A recent study indicated that a mesenchymal profile and expression of CD44 may predict lack of response to sorafenib in HCC patients (39). Although various markers have been studied, identifying predictive biomarkers to sorafenib response remains challenging and warrants further investigation. Our data showed that galectin-1, which had not previously been characterized as having a role in mediating sorafenib resistance, was identified as a protein secreted by HuH-7^R cells. Our mechanistic studies identified galectin-1 as a downstream effector of the AKT/mTOR/HIF-1α pathway. This is consistent with previous study showing that activation of AKT signaling mediates acquired resistance to sorafenib in HCC cells (40) and the constitutive activation of the mTOR pathway in sorafenib-resistant HCC cells by array-based pathway profiling (41). Furthermore, we also showed that down-regulation of galectin-1 suppressed migratory and invasive abilities of HuH-7^R cells, and restored sorafenib sensitivity. Several studies supported that galectin-1 associated with metastatic ability and effects of galectin-1 knockdown on drug sensitivity in different types of cancer (42–44). Taken together, our findings indicate that galectin-1 may be a component of the mechanism that promotes the progression of HCC and resistance to sorafenib. In validation studies using clinical samples, we showed that galectin-1 serum levels were markedly elevated in advanced HCC patients compared with healthy controls; in some cases, galectin-1 serum levels further increased after sorafenib treatment. We also showed that a high serum galectin-1 level was an independent factor associated with poor progress-free survival and overall survival. Additionally, HCC tissue microarray analysis showed that patients with high galectin-1 expression had a higher rate of tumor recurrence and shorter overall survival than those with lower galectin-1 expression (45). Taken together, these data may suggest that the serum levels of galectin-1 can serve as a prognostic factor for HCC. On the other hand, our data support the potential use of galectin-1 serum level as a predictive biomarker of sorafenib treatment, because high galectin-1 serum levels are associated with a low response rate and poor disease control.

In conclusion, we showed that galectin-1 is increased in *in vitro* and *in vivo* sorafenib-resistant HCC models and may promote cancer metastasis and increase tumor invasion. We also showed that high serum galectin-1 levels are associated with poor treatment efficacy and shortened survival in advanced HCC patients treated with sorafenib. These findings support the potential use of galectin-1 as a novel predictive and prognostic biomarker of HCC.

Acknowledgments—We would like to thank the Animal Center of the National Taiwan University College of Medicine for their technical support service.

* This work was supported in part by grants from the Program for Excellence Research Teams of the Ministry of Education and National Research Program for Biopharmaceuticals (NRPB) at the National Science Council (NSC 101-2325-B-002-65 and NSC 102-2325-B-002-061).

S This article contains supplemental Figs. S1 to S6 and Tables S1 to S5.

** To whom correspondence should be addressed: Graduate Institute of Biochemistry and Molecular Biology, College of Medicine, National Taiwan University, No. 1, Jen-Ai Rd, Taipei, Taiwan 100. Tel.: + (886)-2-23123456, ext. 88214; Fax: + (886)-2-23958814; E-mail: chowip@ntu.edu.tw.

REFERENCES

1. Kew, M. C. (2013) Epidemiology of hepatocellular carcinoma in sub-Saharan Africa. *Ann. Hepatol.* **12,** 173–182
2. Bruix, J., and Llovet, J. M. (2002) Prognostic prediction and treatment strategy in hepatocellular carcinoma. *Hepatology* **35,** 519–524
3. Cheng, A. L., Kang, Y. K., Chen, Z., Tsao, C. J., Qin, S., Kim, J. S., Luo, R., Feng, J., Ye, S., Yang, T. S., Xu, J., Sun, Y., Liang, H., Liu, J., Wang, J., Tak, W. Y., Pan, H., Burock, K., Zou, J., Voliotis, D., and Guan, Z. (2009) Efficacy and safety of sorafenib in patients in the Asia-Pacific region with advanced hepatocellular carcinoma: a phase III randomised, double-blind, placebo-controlled trial. *Lancet Oncol.* **10,** 25–34
4. Bruix, J., Sherman, M., and American Association for the Study of Liver, D. (2011) Management of hepatocellular carcinoma: an update. *Hepatology* **53,** 1020–1022
5. Adnane, L., Trail, P. A., Taylor, I., and Wilhelm, S. M. (2006) Sorafenib (BAY 43–9006, Nexavar), a dual-action inhibitor that targets RAF/MEK/ERK pathway in tumor cells and tyrosine kinases VEGFR/PDGFR in tumor vasculature. *Methods Enzymol.* **407,** 597–612
6. Llovet, J. M., Ricci, S., Mazzaferro, V., Hilgard, P., Gane, E., Blanc, J. F., de Oliveira, A. C., Santoro, A., Raoul, J. L., Forner, A., Schwartz, M., Porta, C., Zeuzem, S., Bolondi, L., Greten, T. F., Galle, P. R., Seitz, J. F., Borbath, I., Haussinger, D., Giannaris, T., Shan, M., Moscovici, M., Voliotis, D., Bruix, J., and Group, S. I. S. (2008) Sorafenib in advanced hepatocellular carcinoma. *New Engl. J. Med.* **359,** 378–390
7. Zhou, C., Zhong, Q., Rhodes, L. V., Townley, I., Bratton, M. R., Zhang, Q., Martin, E. C., Elliott, S., Collins-Burow, B. M., Burow, M. E., and Wang, G. (2012) Proteomic analysis of acquired tamoxifen resistance in MCF-7 cells reveals expression signatures associated with enhanced migration. *Breast Cancer Res.* **14,** R45
8. Smith, L., Lind, M. J., Welham, K. J., Cawkwell, L., and Cancer Biology Proteomics, G. (2006) Cancer proteomics and its application to discovery of therapy response markers in human cancer. *Cancer* **107,** 232–241
9. Llovet, J. M., Pena, C. E., Lathia, C. D., Shan, M., Meinhardt, G., Bruix, J., and Group, S. I. S. (2012) Plasma biomarkers as predictors of outcome in patients with advanced hepatocellular carcinoma. *Clin. Cancer Res.* **18,** 2290–2300
10. Ou, D. L., Shen, Y. C., Yu, S. L., Chen, K. F., Yeh, P. Y., Fan, H. H., Feng, W. C., Wang, C. T., Lin, L. I., Hsu, C., and Cheng, A. L. (2010) Induction of DNA damage-inducible gene GADD45beta contributes to sorafenib-induced apoptosis in hepatocellular carcinoma cells. *Cancer Res.* **70,** 9309–9318
11. Zhao, X. Y., Chen, T. T., Xia, L., Guo, M., Xu, Y., Yue, F., Jiang, Y., Chen, G. Q., and Zhao, K. W. (2010) Hypoxia inducible factor-1 mediates expression of galectin-1: the potential role in migration/invasion of colorectal cancer cells. *Carcinogenesis* **31,** 1367–1375
12. Yu, C. C., Yang, J. C., Chang, Y. C., Chuang, J. G., Lin, C. W., Wu, M. S., and Chow, L. P. (2013) VCP phosphorylation-dependent interaction partners prevent apoptosis in Helicobacter pylori-infected gastric epithelial cells. *PLoS One* **8,** e55724
13. Diaz-Gonzalez, J. A., Calvo, F. A., Cortes, J., Garcia-Sabrido, J. L., Gomez-Espi, M., Del Valle, E., Munoz-Jimenez, F., and Alvarez, E. (2006) Prognostic factors for disease-free survival in patients with T3–4 or N+ rectal cancer treated with preoperative chemoradiation therapy, surgery, and intraoperative irradiation. *Int. J. Radiat. Onco. Biol. Phy.* **64,** 1122–1128
14. Yang, W., Cai, Q., Lui, V. W., Everley, P. A., Kim, J., Bhola, N., Quesnelle, K. M., Zetter, B. R., Steen, H., Freeman, M. R., and Grandis, J. R. (2010) Quantitative proteomics analysis reveals molecular networks regulated by epidermal growth factor receptor level in head and neck cancer. *J. Proteome Res.* **9,** 3073–3082
15. Strumberg, D., Richly, H., Hilger, R. A., Schleucher, N., Korfee, S., Tewes, M., Faghih, M., Brendel, E., Voliotis, D., Haase, C. G., Schwartz, B., Awada, A., Voigtmann, R., Scheulen, M. E., and Seeber, S. (2005) Phase I clinical and pharmacokinetic study of the Novel Raf kinase and vascular endothelial growth factor receptor inhibitor BAY 43–9006 in patients with advanced refractory solid tumors. *J. Clin. Oncol.* **23,** 965–972
16. Li, Y. M., Xu, S. C., Li, J., Han, K. Q., Pi, H. F., Zheng, L., Zuo, G. H., Huang, X. B., Li, H. Y., Zhao, H. Z., Yu, Z. P., Zhou, Z., and Liang, P. (2013) Epithelial-mesenchymal transition markers expressed in circulating tumor cells in hepatocellular carcinoma patients with different stages of disease. *Cell Death Dis.* **4,** e831
17. Miow, Q. H., Tan, T. Z., Ye, J., Lau, J. A., Yokomizo, T., Thiery, J. P., and Mori, S. (2014) Epithelial-mesenchymal status renders differential responses to cisplatin in ovarian cancer. *Oncogene* doi:10.1038/onc.2014.136
18. Xie, M., He, C. S., Wei, S. H., and Zhang, L. (2013) Notch-1 contributes to epidermal growth factor receptor tyrosine kinase inhibitor acquired resistance in nonsmall cell lung cancer *in vitro* and *in vivo*. *Eur. J. Cancer* **49,** 3559–3572
19. Tsai, H. C., Su, H. L., Huang, C. Y., Fong, Y. C., Hsu, C. J., and Tang, C. H. (2014) CTGF increases matrix metalloproteinases expression and subsequently promotes tumor metastasis in human osteosarcoma through down-regulating miR-519d. *Oncotarget* **5,** 3800–3812
20. Toiyama, Y., Yasuda, H., Saigusa, S., Tanaka, K., Inoue, Y., Goel, A., and Kusunoki, M. (2013) Increased expression of Slug and Vimentin as novel predictive biomarkers for lymph node metastasis and poor prognosis in colorectal cancer. *Carcinogenesis* **34,** 2548–2557
21. Saito, R., Shirakawa, R., Nishiyama, H., Kobayashi, T., Kawato, M., Kanno, T., Nishizawa, K., Matsui, Y., Ohbayashi, T., Horiguchi, M., Nakamura, T., Ikeda, T., Yamane, K., Nakayama, E., Nakamura, E., Toda, Y., Kimura, T., Kita, T., Ogawa, O., and Horiuchi, H. (2013) Down-regulation of Ral GTPase-activating protein promotes tumor invasion and metastasis of bladder cancer. *Oncogene* **32,** 894–902
22. Hsu, Y. L., Wu, C. Y., Hung, J. Y., Lin, Y. S., Huang, M. S., and Kuo, P. L. (2013) Galectin-1 promotes lung cancer tumor metastasis by potentiating integrin alpha6beta4 and Notch1/Jagged2 signaling pathway. *Carcinogenesis* **34,** 1370–1381
23. Cui, X. D., Lee, M. J., Kim, J. H., Hao, P. P., Liu, L., Yu, G. R., and Kim, D. G. (2013) Activation of mammalian target of rapamycin complex 1 (mTORC1) and Raf/Pyk2 by growth factor-mediated Eph receptor 2 (EphA2) is required for cholangiocarcinoma growth and metastasis. *Hepatology* **57,** 2248–2260
24. Zhou, S., Yi, T., Liu, R., Bian, C., Qi, X., He, X., Wang, K., Li, J., Zhao, X., Huang, C., and Wei, Y. (2012) Proteomics identification of annexin A2 as a key mediator in the metastasis and proangiogenesis of endometrial cells in human adenomyosis. *Mol. Cell. Proteomics* **11,** M112 017988
25. Li, Y., Liang, Q., Wen, Y. Q., Chen, L. L., Wang, L. T., Liu, Y. L., Luo, C. Q., Liang, H. Z., Li, M. T., and Li, Z. (2010) Comparative proteomics analysis of human osteosarcomas and benign tumor of bone. *Cancer Genet. Cytogenet.* **198,** 97–106
26. Hayashi, H., Nabeshima, K., Aoki, M., Hamasaki, M., Enatsu, S., Yamauchi, Y., Yamashita, Y., and Iwasaki, H. (2010) Overexpression of IQGAP1 in advanced colorectal cancer correlates with poor prognosis-critical role in tumor invasion. *Int. J. Cancer* **126,** 2563–2574
27. Garcia-Marcos, M., Jung, B. H., Ear, J., Cabrera, B., Carethers, J. M., and Ghosh, P. (2011) Expression of GIV/Girdin, a metastasis-related protein, predicts patient survival in colon cancer. *FASEB J.* **25,** 590–599
28. de Graauw, M., van Miltenburg, M. H., Schmidt, M. K., Pont, C., Lalai, R., Kartopawiro, J., Pardali, E., Le Devedec, S. E., Smit, V. T., van der Wal, A., Van't Veer, L. J., Cleton-Jansen, A. M., ten Dijke, P., and van de Water, B. (2010) Annexin A1 regulates TGF-beta signaling and promotes metastasis formation of basal-like breast cancer cells. *Proc. Natl. Acad. Sci. U.S.A.* **107,** 6340–6345
29. Guo, C., Liu, S., and Sun, M. Z. (2013) Potential role of Anxa1 in cancer. *Future Oncol.* **9,** 1773–1793
30. Weng, L., Enomoto, A., Ishida-Takagishi, M., Asai, N., and Takahashi, M. (2010) Girding for migratory cues: roles of the Akt substrate Girdin in cancer progression and angiogenesis. *Cancer Sci.* **101,** 836–842
31. White, C. D., Li, Z., Dillon, D. A., and Sacks, D. B. (2011) IQGAP1 protein binds human epidermal growth factor receptor 2 (HER2) and modulates trastuzumab resistance. *J. Biol. Chem.* **286,** 29734–29747
32. Tan, P., Liu, Y., Yu, C., Su, Z., Li, G., Zhou, X., Huang, D., Zhang, X., Qiu, Y., and Tian, Y. (2012) EphA2 silencing in nasopharyngeal carcinoma leads to decreased proliferation, invasion and increased sensitization to paclitaxel. *Onco Lett.* **4,** 429–434
33. Espelt, M. V., Croci, D. O., Bacigalupo, M. L., Carabias, P., Manzi, M., Elola, M. T., Munoz, M. C., Dominici, F. P., Wolfenstein-Todel, C., Rabinovich, G. A., and Troncoso, M. F. (2011) Novel roles of galectin-1 in hepatocellular carcinoma cell adhesion, polarization, and *in vivo* tumor growth. *Hepatology* **53,** 2097–2106
34. Miyahara, K., Nouso, K., Tomoda, T., Kobayashi, S., Hagihara, H., Kuwaki, K., Toshimori, J., Onishi, H., Ikeda, F., Miyake, Y., Nakamura, S., Shiraha, H., Takaki, A., and Yamamoto, K. (2011) Predicting the treatment effect

of sorafenib using serum angiogenesis markers in patients with hepatocellular carcinoma. *J. Gastroen. Hepatol.* **26,** 1604–1611
35. Huang, X. Y., Ke, A. W., Shi, G. M., Zhang, X., Zhang, C., Shi, Y. H., Wang, X. Y., Ding, Z. B., Xiao, Y. S., Yan, J., Qiu, S. J., Fan, J., and Zhou, J. (2013) alphaB-crystallin complexes with 14–3-3zeta to induce epithelial-mesenchymal transition and resistance to sorafenib in hepatocellular carcinoma. *Hepatology* **57,** 2235–2247
36. Arao, T., Ueshima, K., Matsumoto, K., Nagai, T., Kimura, H., Hagiwara, S., Sakurai, T., Haji, S., Kanazawa, A., Hidaka, H., Iso, Y., Kubota, K., Shimada, M., Utsunomiya, T., Hirooka, M., Hiasa, Y., Toyoki, Y., Hakamada, K., Yasui, K., Kumada, T., Toyoda, H., Sato, S., Hisai, H., Kuzuya, T., Tsuchiya, K., Izumi, N., Arii, S., Nishio, K., and Kudo, M. (2013) FGF3/FGF4 amplification and multiple lung metastases in responders to sorafenib in hepatocellular carcinoma. *Hepatology* **57,** 1407–1415
37. Hagiwara, S., Kudo, M., Nagai, T., Inoue, T., Ueshima, K., Nishida, N., Watanabe, T., and Sakurai, T. (2012) Activation of JNK and high expression level of CD133 predict a poor response to sorafenib in hepatocellular carcinoma. *Br. J. Cancer* **106,** 1997–2003
38. Abou-Alfa, G. K., Schwartz, L., Ricci, S., Amadori, D., Santoro, A., Figer, A., De Greve, J., Douillard, J. Y., Lathia, C., Schwartz, B., Taylor, I., Moscovici, M., and Saltz, L. B. (2006) Phase II study of sorafenib in patients with advanced hepatocellular carcinoma. *J. Clin. Oncol.* **24,** 4293–4300
39. Fernando, J., Malfettone, A., Cepeda, E. B., Vilarrasa-Blasi, R., Bertran, E., Raimondi, G., Fabra, A., Alvarez-Barrientos, A., Fernandez-Salguero, P., Fernandez-Rodriguez, C. M., Giannelli, G., Sancho, P., and Fabregat, I. (2015) A mesenchymal-like phenotype and expression of CD44 predict lack of apoptotic response to sorafenib in liver tumor cells. *Int. J. Cancer* **136,** E161–E172
40. Chen, K. F., Chen, H. L., Tai, W. T., Feng, W. C., Hsu, C. H., Chen, P. J., and Cheng, A. L. (2011) Activation of phosphatidylinositol 3-kinase/Akt signaling pathway mediates acquired resistance to sorafenib in hepatocellular carcinoma cells. *J. Pharmacol. Exp. Ther.* **337,** 155–161
41. Masuda, M., Chen, W. Y., Miyanaga, A., Nakamura, Y., Kawasaki, K., Sakuma, T., Ono, M., Chen, C. L., Honda, K., and Yamada, T. (2014) Alternative Mammalian Target of Rapamycin (mTOR) Signal activation in sorafenib-resistant hepatocellular carcinoma cells revealed by array-based pathway profiling. *Mol. Cell. Proteomics* **13,** 1429–1438
42. Chung, L. Y., Tang, S. J., Sun, G. H., Chou, T. Y., Yeh, T. S., Yu, S. L., and Sun, K. H. (2012) Galectin-1 promotes lung cancer progression and chemoresistance by upregulating p38 MAPK, ERK, and cyclooxygenase-2. *Clin. Cancer Res.* **18,** 4037–4047
43. Zhang, P., Zhang, P., Shi, B., Zhou, M., Jiang, H., Zhang, H., Pan, X., Gao, H., Sun, H., and Li, Z. (2014) Galectin-1 overexpression promotes progression and chemoresistance to cisplatin in epithelial ovarian cancer. *Cell Death Dis.* **5,** e991
44. Le Mercier, M., Lefranc, F., Mijatovic, T., Debeir, O., Haibe-Kains, B., Bontempi, G., Decaestecker, C., Kiss, R., and Mathieu, V. (2008) Evidence of galectin-1 involvement in glioma chemoresistance. *Toxicol. Appl. Pharmacol.* **229,** 172–183
45. Wu, H., Chen, P., Liao, R., Li, Y. W., Yi, Y., Wang, J. X., Sun, T. W., Zhou, J., Shi, Y. H., Yang, X. R., Jin, J. J., Cheng, Y. F., Fan, J., and Qiu, S. J. (2012) Overexpression of galectin-1 is associated with poor prognosis in human hepatocellular carcinoma following resection. *J. Gastroenterol. Hepatol.* **27,** 1312–1319